

# Jupiter's X-ray Emission 2007 Part 2: Comparisons with UV and Radio Emissions and In-Situ Solar Wind Measurements

W. R. Dunn<sup>1,2,3</sup>, R. Gray<sup>4</sup>, A. D. Wibisono<sup>1,2</sup>, L. Lamy<sup>5,6</sup>, C. Louis<sup>6,7</sup>, S. V. Badman<sup>4</sup>, G. Branduardi-Raymont<sup>1,2</sup>, R. Elsner<sup>8</sup>, G. R. Gladstone<sup>9</sup>, R. Ebert<sup>9,10</sup>, P. Ford<sup>11</sup>, A. Foster<sup>3</sup>, C. Tao<sup>12</sup>, L. C. Ray<sup>4</sup>, Z. Yao<sup>13</sup>, I. J. Rae<sup>1</sup>, E. J. Bunce<sup>14</sup>, P. Rodriguez<sup>15</sup>, C. M. Jackman<sup>16,17</sup>, G. Nicolaou<sup>1</sup>, J. Clarke<sup>18</sup>, J. Nichols<sup>14</sup>, H. Elliott<sup>6</sup>, R. Kraft<sup>3</sup>

<sup>1</sup>Mullard Space Science Laboratory, Department of Space & Climate Physics, University College London, Holmbury St. Mary, Dorking, Surrey RH5 6NT, UK

<sup>2</sup>The Centre for Planetary Science at UCL/Birkbeck, Gower Street, London, WC1E 6BT, UK

<sup>3</sup>Harvard-Smithsonian Center for Astrophysics, Smithsonian Astrophysical Observatory, Cambridge, 02138, MA, USA

<sup>4</sup>Department of Physics, Lancaster University, Lancaster, LA1 4YW, UK

<sup>5</sup>LESIA, Observatoire de Paris, PSL Research University, CNRS, Sorbonne Universités, UPMC Univ.

Paris 06, Univ. Paris Diderot, Sorbonne Paris Cité, Meudon, France

<sup>6</sup>USN, Observatoire de Paris, CNRS, PSL, UO/OSUC, Nançay, France

<sup>7</sup>IRAP, Université de Toulouse, CNRS, CNES, UPS, Toulouse, France.

<sup>8</sup>ZP12, NASA Marshall Space Flight Center, Huntsville, Alabama, USA

<sup>9</sup>Space Science and Engineering Division, South West Research Institute, San Antonio, Texas, USA

<sup>10</sup>Department of Physics and Astronomy, The University of Texas at San Antonio, San Antonio, Texas, USA

USA

<sup>11</sup>Kavli Institute of Astrophysics and Space Research, MIT, Cambridge, MA, USA

<sup>12</sup>National Institute of Information and Communications Technology, Koganei, Japan

<sup>13</sup>Laboratoire de Physique Atmosphérique et Planétaire, Université de Liège, Liège, B-4000, Belgium

<sup>14</sup>Department of Physics and Astronomy, University of Leicester, Leicester, UK

<sup>15</sup>European Space Astronomy Centre, Madrid, Spain

<sup>16</sup>Department of Physics and Astronomy, University of Southampton, Southampton, SO17 1BJ, UK

<sup>17</sup>Dublin Institute for Advanced Studies, Dublin, Ireland

<sup>18</sup>Center for Space Physics, Boston University, Boston, 02215, MA, USA

## Key Points:

- We characterise 3 types of X-ray aurorae (main oval, ir/regular pulses, flickering aurorae) and compare with radio, UV and solar wind data
- Non-Io decametric bursts occurred with UV auroral brightening, and UV and hard X-ray main auroral emission also brightened contemporaneously
- Soft X-ray aurora was best-fit by iogenic (S,O) spectral lines except during magnetospheric expansion when solar wind ion lines were needed

---

Corresponding author: William R Dunn, w.dunn@ucl.ac.uk

**Abstract**

We compare Chandra and XMM-Newton X-ray observations of Jupiter during 2007 with a rich multi-instrument dataset including: upstream in-situ solar wind measurements from the New Horizons spacecraft, radio emissions from the Nançay Decametric Array and Wind/Waves, and UV observations from the Hubble Space Telescope. New Horizons data revealed two corotating interaction regions (CIRs) impacted Jupiter during these observations. Non-Io decametric bursts and UV emissions brightened together and varied in phase with the CIRs. We characterise 3 types of X-ray aurorae: hard X-ray bremsstrahlung main emission, pulsed/flared soft X-ray emissions and a newly identified dim flickering (varying on short-timescales, but quasi-continuously present) aurora. For most observations, the X-ray aurorae were dominated by pulsed/flaring emissions, with ion spectral lines that were best fit by Iogenic plasma. However, the brightest X-ray aurora was coincident with a magnetosphere expansion. For this observation, the aurorae were produced by both flickering emission and erratic pulses/flares. Auroral spectral models for this observation required the addition of solar wind ions to attain good fits, suggesting solar wind entry into the outer magnetosphere or directly into the pole for this particularly bright observation. X-ray bremsstrahlung from high energy electrons was only bright for one observation, which was during a forward shock. This bremsstrahlung was spatially coincident with bright UV main emission (power > 1 TW) and X-ray ion spectral line dusk emission, suggesting closing of upward and downward current systems during the shock. Otherwise, the bremsstrahlung was dim and UV main emission power was also lower (< 700 GW), suggesting their power scaled together.

**1 Introduction**

Jupiter produces diverse and dynamic multi-waveband auroral emissions. Radio, infrared, visible, ultraviolet and X-ray auroral emissions have all been observed from the planet [e.g. *Badman et al.* [2015]; *Bagenal et al.* [2014] and references therein]. While auroral emissions from the footprints of Jovian satellites [*Kivelson*, 2004; *Saur et al.*, 2004; *Jia et al.*, 2010; *Bonfond et al.*, 2009, 2013; *Bhattacharyya et al.*, 2018; *Zarka*, 1998; *Szalay et al.*, 2018; *Hess et al.*, 2010, 2011] and from low-latitude injection events [*Mauk et al.*, 2002; *Kimura et al.*, 2015] are observed in many wavebands, they are yet to be observed in the X-rays, so we focus on Jupiter’s auroral main emission and the regions poleward of this.

Jupiter’s dominant aurora is its ‘main emission’, which is a near-continuous auroral emission that occurs near the footprints of Ganymede and Callisto [e.g. *Grodent et al.* [2008]]. This bright emission is produced by an upward current system that transfers angular momentum from the planet to plasma in the middle magnetosphere (15-40 Jupiter Radii ( $R_J$ )) in order to enforce corotation [e.g. *Cowley and Bunce* [2001]; *Hill* [2001]]. This upward current system leads electrons to precipitate into Jupiter’s upper atmosphere producing radio, infrared, ultraviolet and hard X-ray bremsstrahlung emissions [summarised in e.g. *Badman et al.* [2015]; *Bagenal et al.* [2014] and references therein].

Poleward of Jupiter’s main emission (mapping beyond 40  $R_J$ ), there are a diverse variety of UV auroral flares, swirls, arcs and dark regions [e.g. *Grodent* [2015] and references therein]. The process that produces most of these is yet to be confirmed. On the dawn-side of the polar aurorae, there is the dark polar region that is seemingly absent of emission but features occasional spots of emission that may relate to reconnection return flows [*Gray et al.*, 2016; *Radioti et al.*, 2011]. In the center of the polar region, there is the ‘swirl region’ from which intermittent pulses of emission are observed, whether or not this is Jupiter’s open field line region is a topic of debate [e.g. *Cowley et al.* [2003]; *Stallard et al.* [2003]; *Vogt et al.* [2015]; *McComas and Bagenal* [2007]; *Cowley et al.* [2008]; *Delamere and Bagenal* [2010]]. Streams of MeV electrons are accelerated away from Jupiter in the swirl region suggesting a source of high acceleration close to the planet [*Paran-*

89 *icas et al.*, 2018], but a connection between these MeV electrons and auroral emissions  
 90 has not yet been identified. Occasionally, long thin auroral arcs or ‘filaments’ bound this  
 91 region centred on noon and may relate to high latitude reconnection [*Nichols et al.*, 2009a].  
 92 In the polar regions between noon and dusk UV and X-ray auroral pulses (or ‘flares’)  
 93 are observed [*Bonfond et al.*, 2011, 2016; *Gladstone et al.*, 2002; *Elsner et al.*, 2005; *Branduardi-*  
 94 *Raymont et al.*, 2008; *Nichols et al.*, 2017a].

95 UV emissions are caused by electron collisions that excite hydrogen in Jupiter’s at-  
 96 mosphere. In contrast, the soft X-ray pulses are dominated by spectral lines from the  
 97 collision of highly charged ions (e.g.  $O^{6+.7+}$ ) with the atmosphere [e.g. *Branduardi-Raymont*  
 98 *et al.* [2004, 2007]]. These lines are produced when ions collide with atmospheric neu-  
 99 trals and charge exchange to take an electron from a neutral and consequently emit an  
 100 X-ray photon [*Cravens et al.*, 1995]. If the precipitating ions are of a magnetospheric ori-  
 101 gin then they will be only singly or doubly charged (e.g.  $O^{+.2+}$ ) and must therefore un-  
 102 dergo a series of high energy ( $> 0.5$  MeV/u) collisions that strip electrons from them be-  
 103 fore they are of a sufficiently high charge state (e.g.  $O^{6+.7+}$ ) to produce the observed  
 104 X-ray spectral lines [*Houston et al.*, 2018; *Houston et al.*]. *Clark et al.* [2017] have shown  
 105 that large potential drops do exist over Jupiter’s pole, which may provide at least part  
 106 of the ion acceleration to produce the observed X-rays. Alternatively, solar wind ions al-  
 107 ready exist in a sufficiently high charge state, but would require extremely large currents  
 108 ( $\sim$ MA) in order to provide large enough ion fluxes for the X-ray spectral lines observed  
 109 [*Cravens et al.*, 2003].

110 A variety of processes have been proposed to explain the precipitation of X-ray-  
 111 producing ions in the polar region including: downward current systems in the outer mag-  
 112 netosphere that complete the upward corotation enforcement system [*Cravens et al.*, 2003],  
 113 dayside reconnection and/or cusp processes [*Bunce et al.*, 2004; *Pallier and Prangé*, 2001,  
 114 2004], Kelvin Helmholtz Instabilities [*Kimura et al.*, 2016; *Dunn et al.*, 2016, 2017], rotation-  
 115 driven reconnection in the outer magnetosphere [*Guo et al.*, 2018a,b; *Yao et al.*, 2017]  
 116 and/or a combination of wave processes [e.g. *Manners et al.* [2018]]. The source for au-  
 117 roral flares near regions mapping to the magnetopause suggests that the emission may  
 118 be diagnostic of the relationship between Jupiter’s magnetosphere and the solar wind.

## 119 1.1 Connections Between the Aurora and the Solar Wind

120 Jupiter’s auroral response to changes in solar wind pressure has been studied us-  
 121 ing a variety of wavebands and theoretical arguments [e.g. *Prangé et al.* [1993]; *Baron et al.*  
 122 [1996]; *Zarka* [1998]; *Southwood and Kivelson* [2001]; *Cowley and Bunce* [2001]; *Chané*  
 123 *et al.* [2017]; *Sinclair et al.* [2019]]. *Clarke et al.* [2009] and *Nichols et al.* [2009b] showed  
 124 that the UV main emission brightens and thickens in response to solar wind shocks. *Bad-*  
 125 *man et al.* [2016] showed that the inverse is also true and that magnetospheric expan-  
 126 sion leads the main emission to dim and shift to lower latitudes, through reduced elec-  
 127 tron density and thermal energy or increased inward (outward) transport of hot (cold)  
 128 plasma. *Nichols et al.* [2017a] also showed that solar wind compressions can trigger puls-  
 129 ing arcs of UV emission in the dusk sector, which may relate to tail reconnection or ve-  
 130 locity shears. *Kita et al.* [2016] have shown that not only does the UV auroral bright-  
 131 ness vary with solar wind conditions but that there is a correlation between the total au-  
 132 roral power and the length of the quiescent interval that preceded the solar wind shock.  
 133 *Grodent et al.* [2018] analysed an extensive Hubble Space Telescope (HST) campaign to  
 134 identify several classes of auroral behaviour of which they characterise one that is driven  
 135 by external conditions.

136 Jovian radio emissions can also be triggered by solar wind conditions and can there-  
 137 fore be used as a proxy for compressions/rarefactions [*Gurnett et al.*, 2002; *Prangé et al.*,  
 138 2004; *Lamy et al.*, 2012; *Hess et al.*, 2012, 2014; *Dunn et al.*, 2016; *Desch and Barrow*,  
 139 1984; *Echer et al.*, 2010]. *Hess et al.* [2012, 2014] in particular showed that forward and

140 reverse solar wind shocks can be distinguished through differing time-frequency morphol-  
 141 ogy of bursts of Jovian non-Io Decametric emission, namely the rise of duskside and dawn-  
 142 side/duskside sources, respectively.

143 X-ray emissions from Jupiter have also exhibited a solar wind relationship, but this  
 144 is less well catalogued than for the radio and UV. *Branduardi-Raymont et al.* [2007] noted  
 145 that X-ray emissions increased during an interval of pronounced solar activity. *Dunn et al.*  
 146 [2016] found significant changes in the spatial, spectral and temporal trends of Jupiter's  
 147 aurora between an observation during an Interplanetary Coronal Mass Ejection (ICME)  
 148 impact and an observation during ICME recovery. *Kimura et al.* [2016] found correla-  
 149 tions between solar wind velocity and the X-ray emissions. In the absence of upstream  
 150 solar wind measurements, both *Dunn et al.* [2016] and *Kimura et al.* [2016] propagated  
 151 solar wind conditions from measurements at 1 AU to Jupiter at  $\sim 5$  AU. These propa-  
 152 gation models had large timing uncertainties ( $\pm 10$  - 15 hours in *Dunn et al.* [2016] and  
 153  $\pm 48$  hours in *Kimura et al.* [2016]) and this may have at least partially lead to the two  
 154 works contradictory results, in which the former suggests a connection with solar wind  
 155 density but not velocity and the latter with velocity, but not density. This present study  
 156 provides a rare opportunity to examine contemporaneous auroral data with solar wind  
 157 information from an upstream monitor.

## 158 1.2 Connections Between Different Auroral Wavebands

159 Leveraging the UV and X-ray wavebands together lets one utilise the high-photon  
 160 counts observed by HST (typically for *sim40* mins at a time) in partnership with the longer  
 161 duration (up to 40 hours), but lower count rate X-ray observations by Chandra or XMM-  
 162 Newton. A single overlapping observation has produced two important findings: at least  
 163 some UV and X-ray auroral flares are coincident (within a few 1000 km) [*Elsner et al.*,  
 164 2005] and the UV main emission is coincident with the X-ray electron bremsstrahlung  
 165 emission [*Branduardi-Raymont et al.*, 2008].

166 Quasi-periodic flaring has also been observed in the UV polar aurora and main emis-  
 167 sion with periods of a few to 10 minutes [*Bonfond et al.*, 2011, 2016; *Nichols et al.*, 2017a,b].  
 168 The 40 min duration of HST observations means regular pulsations with a longer inter-  
 169 pulse time than this would be difficult to identify, however, the several hour X-ray ob-  
 170 servations have detected regular pulses of 8-45 minutes in  $\sim 10$  observations [*Gladstone*  
 171 *et al.*, 2002; *Dunn et al.*, 2016; *Jackman et al.*, 2018]. For most other observations the  
 172 X-ray aurora still pulses, but these pulses are more erratic and the poles sometimes be-  
 173 have independently and sometime pulse in tandem [*Dunn et al.*, 2017]. Recent observa-  
 174 tions in the infrared have also revealed emissions poleward of the UV main emission that  
 175 pulsed on timescales of 10 minutes [*Watanabe et al.*, 2018].

176 Periodic radio pulsations also occur with similar characteristic periods to the X-  
 177 ray pulses and may be produced by electrons streaming away from the planet [*MacDowall*  
 178 *et al.*, 1993]. Bursts of non-Io decametric radio emission have also been observed to oc-  
 179 cur contemporaneously with significant brightening of the X-ray aurora [*Dunn et al.*, 2016].

180 Through February and March 2007, NASA's New Horizons spacecraft was approach-  
 181 ing Jupiter. At this time, a series of HST, Chandra and XMM-Newton observations of  
 182 Jupiter were conducted, while radio observations by Wind/Waves and the NDA (Nançay  
 183 Decameter Array) were ongoing. The combination of these campaigns provides a rich  
 184 multi-waveband dataset. In this paper, we utilise this data to explore links between Jo-  
 185 vian X-ray emissions, other aurora wavebands and the solar wind. This is the second in  
 186 a series of papers that include the Jovian X-ray data from 2007. The first paper [*Dunn*  
 187 *et al.*, in review] reported general trends in the equatorial and auroral X-ray emissions  
 188 during solar minimum.

Instrument	Date	Time (UT)	DOY	CML (°)	Aurora (N/S)	General SW Conditions
CXO	8 Feb	08:31 - 13:47	39	94 - 286	N	CIR Day 4
CXO	10-11 Feb	19:54 - 01:21	41-42	88 - 286	N	Rarefaction
HST	21 Feb	15:21 - 16:04	52	141 - 167	N	Rarefaction
HST	22 Feb	11:12 - 11:14	53	141 - 142	N	Rarefaction
HST	23 Feb	08:56 - 09:05	54	209 - 215	N	CIR Arrival
HST	24 Feb	12:50 - 14:25	55	141 - 198	N	CIR Day 2
CXO	24-25 Feb	21:24 - 02:17	55-56	90 - 267	N	CIR Day 2
XMM	24-25 Feb	20:14 - 03:02	55-56	47 - 294	N	CIR Day 2
HST	26 Feb	15:17 - 15:59	57	171 - 197	N	CIR Day 3
HST	27 Feb	10:29 - 11:11	58	147 - 173	N	CIR Day 4/Rarefaction
HST	2 Mar	07:46 - 09:13	61	140 - 193	N	Rarefaction
HST	3 Mar	04:05 - 05:45	62	157 - 218	N	Rarefaction
CXO	3 Mar	07:43 - 13:03	62	286 - 120	S	Rarefaction or CIR Arrival
XMM	3 Mar	07:17 - 14:42	62	271 - 180	S	Rarefaction or CIR Arrival
HST	4 Mar	10:24 - 11:06	63	177 - 202	N	CIR Arrival
HST	5 Mar	05:35 - 06:18	64	153 - 179	N	CIR Day 2
HST	6 Mar	11:01 - 11:05	65	140 - 143	N	CIR Day 3
CXO	7 Mar	14:19 - 19:08	66	48 - 223	~N	CIR Day 4/Rarefaction
XMM	7 Mar	12:52 - 20:21	66	356 - 267	S→N	CIR Day 4/Rarefaction
CXO	8-9 Mar	21:04 - 02:45	67-68	83 - 290	N	Rarefaction
XMM	8-9 Mar	19:50 - 02:20	67-68	39 - 275	N	Rarefaction
HST	9 Mar	09:10 - 10:38	68	164 - 218	N	Rarefaction
HST	10 Mar	04:29 - 04:39	69	146 - 151	N	Rarefaction

199 **Table 1.** Table of Jupiter observations dates and times and Central Meridian Longitude  
200 (CML) ranges during Chandra (CXO), XMM-Newton (XMM) and Hubble Space Telescope  
201 (HST) observations in February and March 2007. Fig 1 and 2 are interpreted to provide in-  
202 stances of solar wind rarefactions and compressions from corotating interaction regions (CIR) for  
203 each observation.

189 In this work, we begin by introducing the February and March 2007 remote obser-  
190 vation campaigns (section 2). We then present the New Horizons solar wind measure-  
191 ments (section 3) and the more thoroughly studied UV (section 4) and radio (section 5)  
192 wavebands to provide further context for the X-ray emissions. Having built an under-  
193 standing of the conditions, we present the variation in X-ray spectra (section 6), spatial  
194 morphology (section 7) and temporal signatures (section 8) from observation to obser-  
195 vation. We close by connecting the different X-ray auroral behaviours with the solar wind  
196 and multi-waveband observations (section 9 and 10).

## 197 2 February and March 2007 Remote Observations of Jupiter

### 198 2.1 Chandra and XMM-Newton X-ray Campaign

204 Through February and March 2007 a series of Jupiter X-ray observations were con-  
205 ducted with Chandra's ACIS instrument and with the XMM-Newton Observatory. The  
206 X-ray observations were shorter than other Jovian X-ray campaigns lasting  $\sim 0.5$  Jupiter  
207 rotations each. Jupiter's sub-observer latitude was  $-3.31^\circ$ , so the Northern geographic  
208 pole was slightly obscured. The observation times and associated longitude ranges are  
209 listed in Table 1. Unlike Earth's aurora, Jupiter's main auroral emission is fixed in plan-  
210 etary (System III - S3) longitude and thus rotates with the planet. The dipole tilt means  
211 that the longitude locations are different for each pole. For the North, the aurorae are

212 more strongly offset from the spin axis and mostly situated between  $\sim 140\text{-}270^\circ$  S3 lon-  
 213 gitude and above  $55^\circ$  latitude. The Southern aurorae are more closely aligned to the spin  
 214 axis, but still feature an offset with a viewing preference from  $\sim 300\text{-}120^\circ$  longitude and  
 215 above  $60^\circ$  latitude. Table 1 therefore shows that the observations on 8th, 10-11th, 24-  
 216 25th February and 8-9th March provided coverage of the Northern aurora, while 3rd March  
 217 covered the Southern aurora (and is discussed in *Dunn et al.* [2017]) and 7th March cov-  
 218 vered a transition between the two. For all Chandra observations, the combination of red-  
 219 leak through the ACIS Optical Blocking Filter and contaminant build-up had to be ac-  
 220 counted for in the manner described in *Elsner et al.* [2005] and *Dunn et al.* [2017].

## 221 2.2 UV Observation Campaign

222 From the 20th February to the 10th of March 2007 (inclusive), there was an ex-  
 223 tensive HST UV observing campaign with the Advanced Camera for Surveys Solar Blind  
 224 Channel. This consisted of 907 (580) UV images of the Northern (Southern) Aurora, taken  
 225 in groups of 15 images spanning  $<1$  hour, with most exposures lasting  $\sim 100$  s (discussed  
 226 in detail in *Clarke et al.* [2009]; *Nichols et al.* [2009b] and *Stallard et al.* [2016]). Table  
 227 1 show the UV observations contemporaneous to the X-ray observations.

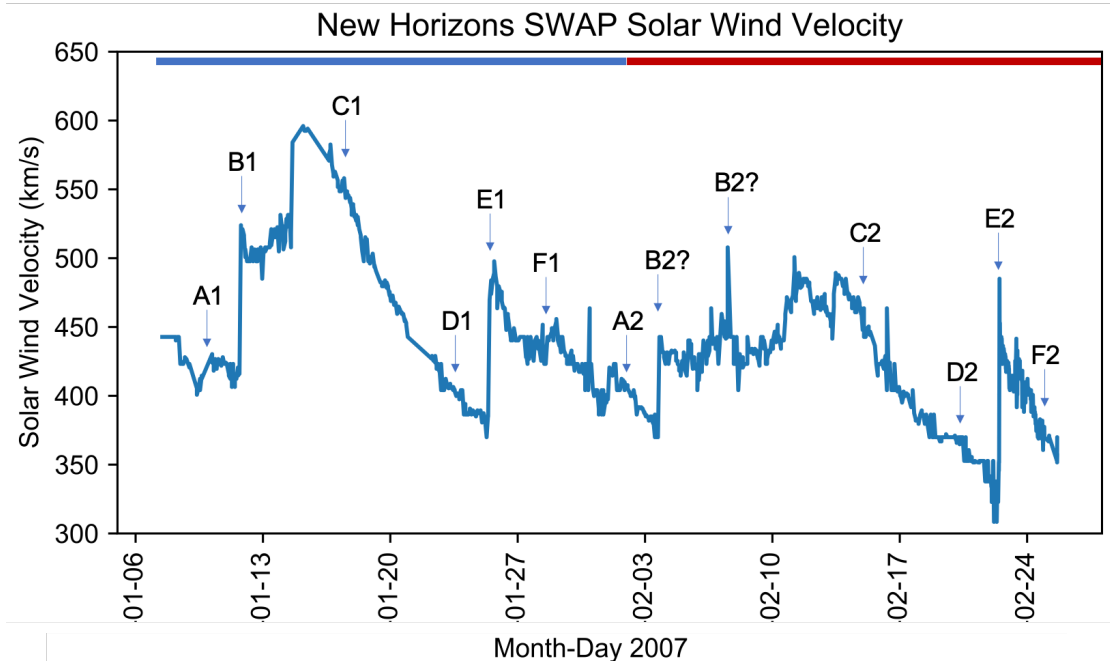
## 228 2.3 Radio Observation Campaign

229 Since 1977, the NDA has observed Jupiter radio emissions for  $\sim 8$  hours per day  
 230 between 10-40 MHz (*Boischoit et al.* [1980]; *Lecacheux* [2000]; *Lamy et al.* [2017]; [www.obs-](http://www.obs-nancay.fr)  
 231 [nancay.fr](http://www.obs-nancay.fr)). The NDA measurements obtained with its Routine receiver display a good  
 232 time-frequency resolution (1s x 75 kHz) while its polarization capability enables one to  
 233 disentangle the hemisphere of origin of decametric extraordinary mode emission (RH or  
 234 LH polarized when emitted from the northern or southern hemisphere respectively). These  
 235 capabilities allowed *Marques et al.* [2017] to conduct a statistical analysis of radio emis-  
 236 sions from Jupiter and generate a catalogue of these emissions. We list the non-Io arcs  
 237 from their catalogue in Table 2.

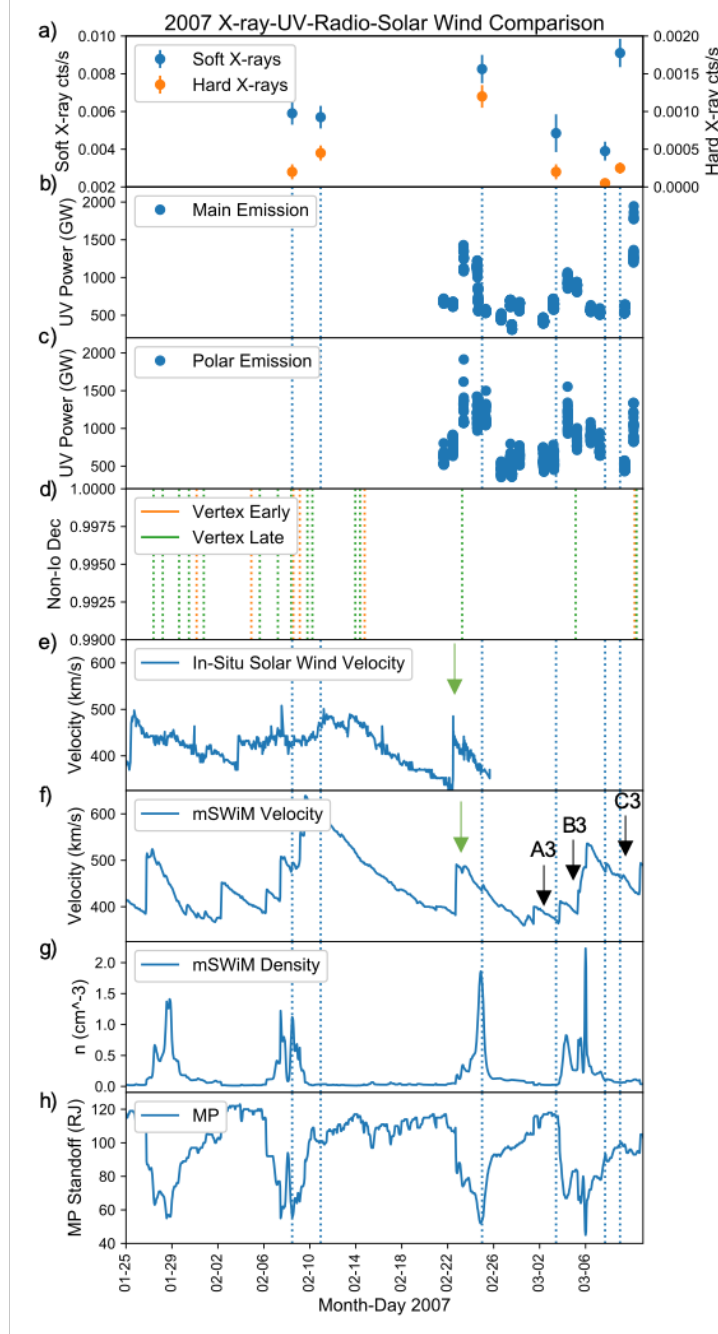
238 The WIND spacecraft has operated since 1993. Its Waves instrument measures ra-  
 239 dio emission from a few Hz to 14 MHz [*Bougeret et al.*, 1995] and provides quasi-continuous  
 240 measurements at moderate time-frequency resolution (60s x 50 kHz in this study) so that  
 241 while it is designed to track solar radio bursts, it is sensitive enough to remotely detect  
 242 emissions from Jupiter (and other radio sources).

## 243 3 New Horizons Solar Wind Measurements

244 On February 26th 2007, New Horizons entered Jupiter’s magnetosphere for a Jupiter  
 245 flyby. Prior to this, the Solar Wind Around Pluto (SWAP) instrument [*McComas et al.*,  
 246 2008] measured the solar wind conditions upstream of Jupiter. From the 8th Feb onwards,  
 247 there was a propagation time between New Horizons and the Jovian bow shock of be-  
 248 tween a few hours and 19 hours (depending on the specific solar wind conditions at that  
 249 time, the magnetosphere extent and the New Horizons-bow shock distance). SWAP is  
 250 built for the more rarified solar wind conditions near the orbit of Pluto [*Bagenal et al.*,  
 251 2016; *McComas et al.*, 2016; *Elliott et al.*, 2016, 2018; *McComas et al.*, 2007] but has been  
 252 used successfully to study the Jovian magnetotail [*Ebert et al.*, 2010], magnetosheath [*Nico-*  
 253 *laou et al.*, 2014], magnetotail boundary layer [*Nicolaou et al.*, 2015] and the solar wind  
 254 at various locations in the heliosphere [*Elliott et al.*, 2016, 2019]. Figure 1 shows the SWAP  
 255 estimates of the solar wind velocity upstream of Jupiter from Jan 10th to Feb 26th, 2007.  
 256 This was during an extended solar minimum, when solar wind structures are expected  
 257 to be well organised with solar rotation and ICMEs would be rare [e.g. *Owens and Forsyth*  
 258 [2013]].



259 **Figure 1.** Solar wind velocities upstream of Jupiter as measured by the New Horizons SWAP  
 260 instrument from 6th January to 26th February 2007 (inclusive). ABC and DEF indicate two  
 261 distinct corotating interaction regions which impact Jupiter multiple times during this interval.  
 262 Each interval when they impact Jupiter is indicated by their numbering (e.g. B1 indicates the  
 263 first arrival of the shock B at Jupiter; E2 indicates the second arrival of shock E ). New Horizons  
 264 passed into Jupiter's magnetosphere on 26th Feb. Alternating blue and red bars at the top of the  
 265 plot indicate solar rotations.



266 **Figure 2.** Multi-waveband comparisons with solar wind conditions. a) Chandra ACIS North-  
 267 ern aurora soft and hard X-ray counts per second for each observation (tracked through subse-  
 268 quent panels by blue dotted lines). Total power for the b) UV main aurora and c) polar aurora  
 269 from HST. d) Times of non-Io vertex early (orange) and late (green) emissions (Table 2). e)  
 270 New Horizons SWAP Solar Wind Peak Velocity upstream of Jupiter. mSWiM propagations  
 271 from 1 AU of solar wind velocity (f), density (g) and mSWiM dynamic pressure driven *Joy et al.*  
 272 [2002] model magnetopause stand-off distances (h). f, g and h have been shifted so that the ve-  
 273 locity discontinuity E2 in the SWAP and mSWiM velocities is aligned (vertical green arrow),  
 274 and so that the arrival of shock ABC occurs a solar rotation later than observed by New Hor-  
 275 zons at A3B3C3, which coincides with the UV auroral morphology change. As shown by *Nichols*  
 276 *et al.* [2009b] and through auroral comparisons with New Horizons in-situ data, the shift in the  
 277 mSWiM data is not constant but varies for CIR ABC vs CIR DEF. We interpret the X-ray data  
 278 assuming different shifts for each CIR. Un-shifted data is shown in the supporting information.



279 Figure 1 shows several solar wind structures labelled alphabetically. Their recur-  
 280 rence with solar rotation is indicated numerically, so that the structures ABC and DEF  
 281 recur each solar rotation. A and D indicate slow quiescent solar wind prior to a shock.  
 282 B and E indicate the arrival of a shock that recurs approximately every solar rotation.  
 283 C and F show the declines from fast solar wind through to slower solar wind. We inter-  
 284 pret the shocks at B and E as co-rotating interaction regions (CIRs). A CIR occurs where  
 285 slow solar wind (e.g. A1) is caught-up by fast solar wind. The fast wind (e.g. C1) is slowed  
 286 at the shock (e.g. B1) where the populations meet and the solar wind density increases  
 287 in this region. These density increases will act to compress Jupiter’s magnetosphere. The  
 288 shocked fast wind then passes New Horizons and SWAP measures fast un-shocked so-  
 289 lar wind (e.g. C1), which then transitions to slow wind across a rarefaction (e.g. C1 to  
 290 D1) [for CIR details see e.g. *Owens and Forsyth* [2013] and references therein]. As the  
 291 shock passes Jupiter and the density decreases, Jupiter’s magnetosphere will expand. These  
 292 CIRs recur with solar rotation (e.g. D2-E2-F2 is one solar rotation after D1-E1-F1) and  
 293 their consequent compressions and expansions of Jupiter’s magnetosphere are also ex-  
 294 pected to recur. For further inspection of the solar wind evolution measured by New Hori-  
 295 zons SWAP instrument in this interval see the supporting information.

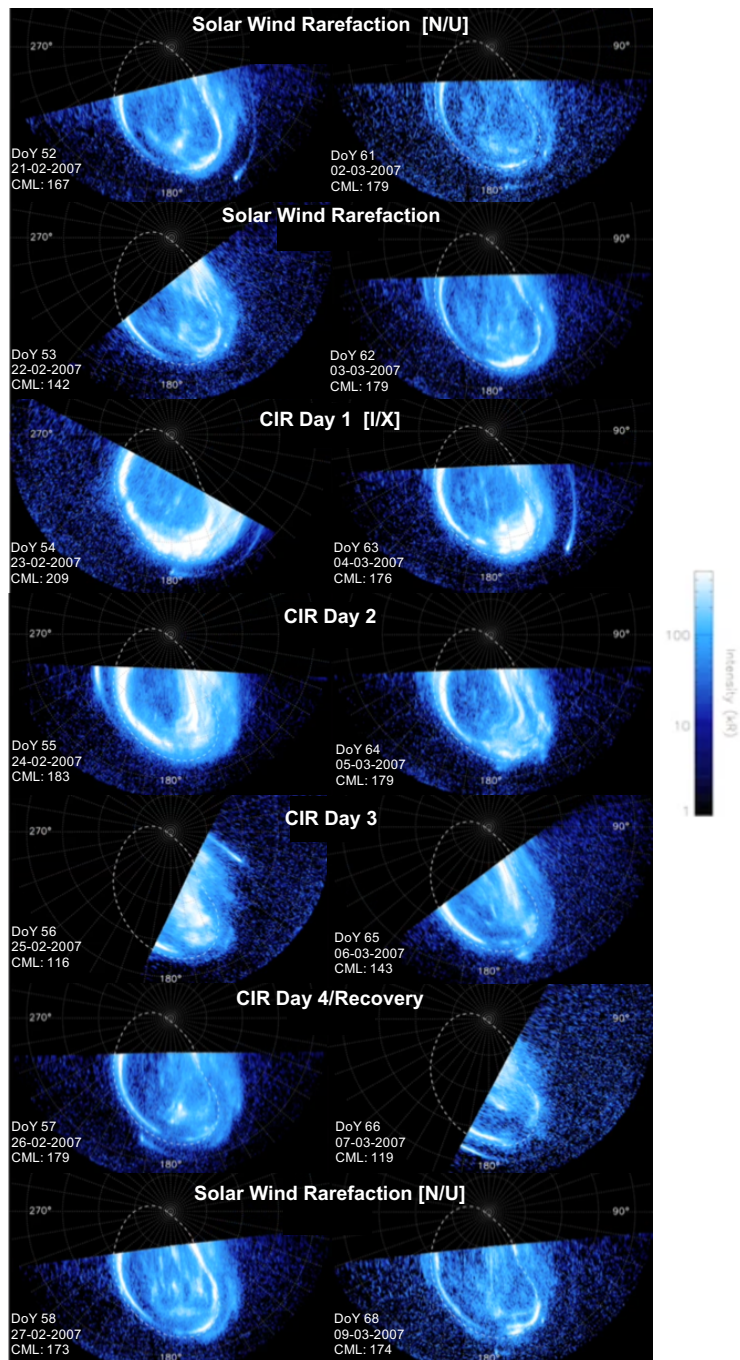
296 SWAP provided solar wind velocity measurements upstream of Jupiter for only 3  
 297 of the X-ray observations before passing into Jupiter’s magnetosphere. We attempted  
 298 to leverage the SWAP measurements to further interpret the subsequent 3 observations  
 299 by: a) searching for signatures that repeated with solar rotation to predict the recurrence  
 300 of compressions/expansions from e.g. corotating interaction regions and b) using SWAP  
 301 to validate propagated solar wind conditions from 1 AU using the mSWiM [*Zieger and*  
 302 *Hansen*, 2008] and Tao models [*Tao et al.*, 2005], which provided insight into the solar  
 303 wind density which could not be derived from the SWAP data. For example, New Hori-  
 304 zons passed into Jupiter’s magnetosphere before being able to measure the third recur-  
 305 rence of CIR A-B-C (A3-B3-C3). Assuming recurrence with solar rotation, the shock B3  
 306 should recur on DOY 62-63 (March 3rd-4th) (see Fig. 1 and 2).

307 During this campaign, Jupiter was 3-4 months from opposition (5th June 2007),  
 308 so propagation models were particularly unreliable (uncertainties  $\sim 2$  days), we there-  
 309 fore utilised them cautiously. The propagation models do show the same recurring CIRs  
 310 and associated shocks as the New Horizons data, but there are differing time shifts be-  
 311 tween the models and in-situ arrival of the two shocks (also found by *Nichols et al.* [2009b]).  
 312 To utilise the density propagations, we shift the propagation by +1 days, to align the  
 313 SWAP peak in solar wind velocity at E2 with the same mSWiM velocity peak (green ar-  
 314 row on Fig. 2e and f), then -1 days to bring the CIR A3-B3-C3 in line with its expected  
 315 arrival from the SWAP data (Fig. 2f) and UV auroral morphology change. For consis-  
 316 tency with *Nichols et al.* [2009b], we show mSWiM in the main text (Fig.2), but there  
 317 is good agreement between the Tao model and the complete unshifted propagations from  
 318 1 AU are shown in the supporting information.

319 Combining the density propagations with the solar wind velocity provides insight  
 320 into the dynamic pressure experienced by Jupiter. In combination with the *Joy et al.*  
 321 [2002] model, this estimates the magnetopause standoff distance as shown in Fig. 2h.

## 322 4 UV Observation Analysis

330 The 2007 UV aurorae are analysed in detail in *Nichols et al.* [2009b]; *Clarke et al.*  
 331 [2009] and *Stallard et al.* [2016]. Figure 2b and c reproduce the UV auroral powers shown  
 332 in *Nichols et al.* [2009b], updating these for kR/power conversion factors for an absorbed  
 333 to unabsorbed color ratio of 2.5 as discussed in *Gustin et al.* [2012]. Comparing these  
 334 powers with the X-ray emissions in fig 2a shows that the Northern auroral hard X-ray  
 335 emission appears to only be significant for UV main emission powers greater than 1 TW.



323 **Figure 3.** UV Auroral Images as close to CML  $180^\circ$  as possible. These show the auroral morphology in phase from solar wind rarefaction through the two CIR induced shocks (D2-E2-F2  
 324 from Fig 1 in the left column and A3-B3-C3 from Fig 1 in the right column) and back to rarefied solar wind. In square brackets are the *Grodent et al.* [2018] categories of UV auroral morphology  
 325 indicating the start times of Narrow/Unsettled [N/U] morphology and Injection/eXternal perturbation morphology [I/X] and the subsequent evolution through these states. Each image is a  $\sim 2$   
 326 minute exposure. Images are reproduced from supporting information from *Nichols et al.* [2009b].  
 327  
 328  
 329

336 For the other X-ray observations the hard X-ray emission is below 0.0005 counts/second  
 337 and the contemporaneous UV main emission is less than 700 GW.

338 Comparing the power variations with the incidence of solar wind compressions (Fig  
 339 2h) shows the correlation between UV auroral power and compressions of the magne-  
 340 tosphere. In Figure 3, we show that the UV aurora also clearly exhibits very similar mor-  
 341 phological responses in phase with the evolution of both CIR D2-E2-F2 and A3-B3-C3.

342 Prior to the CIR (21st-22nd Feb and 2nd-3rd March), the main oval is thin and  
 343 occurs along the dashed average location contour defined by *Nichols et al.* [2009b]. There  
 344 are intermittent ‘swirls’ of emission in the high latitude swirl region and bright flashes/flares  
 345 from what Pallier and Prange (2004) describe as the cusp spot. When the CIRs arrive  
 346 (23rd Feb and 4th March), the main oval significantly thickens and moves poleward on  
 347 the dawn side. From noon-dusk the main emission is found at higher latitudes. This po-  
 348 lar dusk arc emits bright pulses 20-30 minutes apart. On 4th March ‘the cusp spot’ is  
 349 still observed through bright flashes. One day after the shock arrival (24th Feb and 5th  
 350 March), the thick polar dusk arc splits into multiple arcs, which exhibit pulsations at  
 351 their equatorial edge and bifurcate into extensions across the polar region. Two days af-  
 352 ter the shock arrival (25th Feb, 6th March), bright flares continue to be produced. For  
 353 6th March, there are no longer discrete arcs, only a single thick and pulsing arc. Upwards  
 354 of three days after the CIR the solar wind returns to rarefied conditions (26-27th Feb,  
 355 7-9th March) and Jupiter’s magnetosphere would be expected to expand. The main oval  
 356 responds to this by dimming and returning to lower latitudes, while the polar emissions  
 357 shifts to sporadic pulses across a broader polar region.

358 Using the classification of auroral morphologies defined by *Grodent et al.* [2018],  
 359 the images evolve from ‘Narrow’/‘Unsettled’ at the beginning of each interval, through  
 360 to ‘Injections/eXternal perturbation’ during the CIR compressions and returning to ‘Nar-  
 361 row/Unsettled’ in the recovery and rarefaction intervals.

## 362 5 Radio Observation Analysis

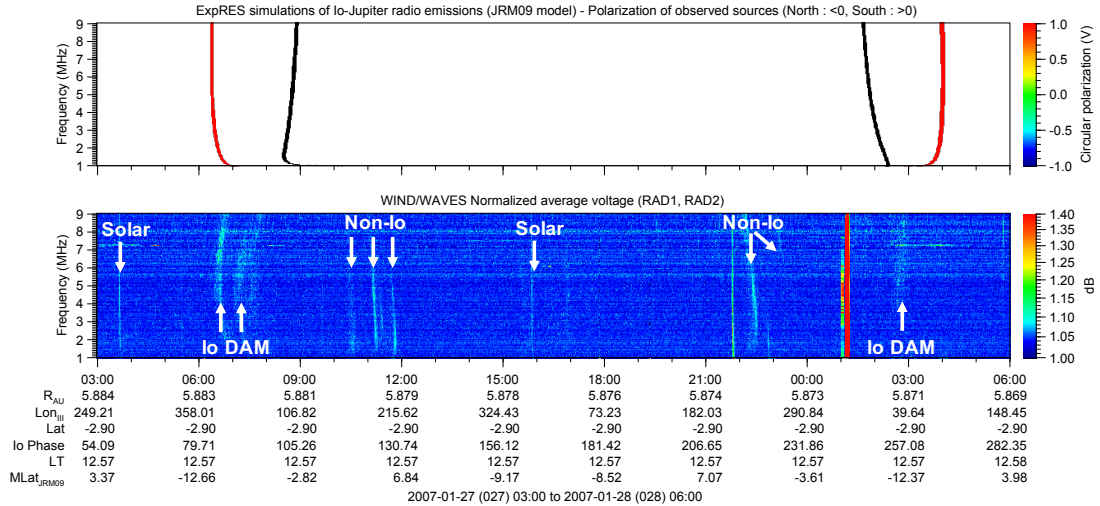
363 *Hess et al.* [2012, 2014] showed that non-Io bursts of decametric emission (DAM)  
 364 are triggered by solar wind compressions or rarefactions. Expansions of the magne-  
 365 tosphere trigger DAM with both vertex early (similar to an opening parenthesis) and ver-  
 366 tex late (a closing parenthesis) morphology, while compressions only trigger vertex late  
 367 DAM emission. The shape of these arcs results from the combination of the motion of  
 368 the source with respect to the observer and the hollow-conical shape of the structure (see  
 369 e.g. *Hess et al.* [2014] for more details).

374 Using the catalogue produced by *Marques et al.* [2017] and by surveying the Wind/Waves  
 375 (1-15 MHz) measurements, we collated the non-Io decametric emissions from January  
 376 to March 2007 (Table 2). We filtered out the DAM arcs produced by the Io-Jupiter in-  
 377 teraction through ExPRES simulations [detailed in *Hess et al.* [2008]; *Louis et al.* [2017]  
 378 and *Louis, C. K. et al.* [2019]]. The Wind/Waves spectrograms and ExPRES simulations  
 379 for Table 2 can be found in the supporting information. We disregarded the WIND/Waves  
 380 data between 9.5-15 MHz due to extensive Radio Frequency Interference bands.

381 Figure 4 shows an example of an interval that shows both types of emission on 27  
 382 Jan 2007. Fig 4b shows that between 07:00-08:00 (DOY 27 2007) and 02:00-03:00 (DOY  
 383 28 2007) the decametric arcs observed at less than 9 MHz by Wind/Waves are a good  
 384 fit to the simulated vertex early and vertex late Io arcs shown in Fig 4a. Fig 4b also shows  
 385 decametric arcs between 10:00-12:00 that cannot be attributed to Io (Fig 4a) and are  
 386 of the vertex-late morphology associated with solar wind compressions [*Hess et al.*, 2012,  
 387 2014]. Indeed, the in-situ solar wind data shows that solar wind compression E1 occurred  
 388 within 1 Jupiter rotation of this burst, suggesting a connection between the two. Ad-  
 389 ditional bursts of decametric emission occur  $\sim$ 12 hours after these bursts between 22:00

Date - Time	Vertex Early/Late	Instrument (NDA/WAV)
27 Jan 08:00 - 08:07	Late	NDA
27 Jan 08:25 - 08:32	Late	NDA
27 Jan 09:30 - 12:00	Late	WAV
27 Jan 21:00 - 23:55	Late	WAV
28 Jan 04:42 - 05:03	Late	NDA
28 Jan 17:00 - 18:00	Late	WAV
29 Jan 14:30 - 15:45	Late	WAV
30 Jan 11:00 - 12:00	Late	WAV
31 Jan 03:00 - 04:00	Early	WAV
31 Jan 17:00 - 18:00	Late	WAV
4 Feb 21:30 - 22:00	Early	WAV
5 Feb 09:00 - 10:00	Late	WAV
5 Feb 15:30 - 16:30	Late	WAV
5 Feb 19:00 - 20:00	Late	WAV
7 Feb 05:11 - 05:35	Late	NDA
8 Feb 03:00 - 04:00	Late	WAV
8 Feb 13:00 - 14:00	Early	WAV
9 Feb 02:50 - 03:10	Early	WAV
9 Feb 06:00 - 07:00	Late	WAV
9 Feb 19:00 - 20:00	Late	WAV
10 Feb 04:59 - 05:24	Late	NDA
13 Feb 22:30 - 23:30	Late	WAV
14 Feb 08:30 - 09:30	Late	WAV
14 Feb 18:00 - 19:00	Early	WAV
23 Feb 05:30 - 07:00	Late	WAV
5 Mar 03:09 - 03:22	Late	NDA
10 Mar 05:30 - 07:30	Early	WAV
10 Mar 09:30 - 11:30	Late	WAV

370 **Table 2.** Table of detected Non-Io Decametric Emissions from Jupiter by the NDA and  
371 WIND/WAV instruments from 27 Jan - 10 March 2007. NDA Measurements are from the *Mar-*  
372 *ques et al.* [2017] catalogue of decametric emissions. The early or late morphology from *Hess*  
373 *et al.* [2014] for each non-Io decametric arc is listed.



392 **Figure 4.** a) ExpRES radio spectrogram simulations of Northern (black) and Southern (red)  
 393 Io-DAM arcs (for details see *Louis et al.* [2017]; *Louis, C. K. et al.* [2019]) observed on 27th-  
 394 28th January 2007, and b) radio spectrograms recorded by the WAVES instrument on the Wind  
 395 spacecraft (total flux density). ExpRES simulates the times and morphology of the radio emis-  
 396 sions from Io, which through comparison with the Wind/Waves data permits identification of the  
 397 Io and Non-Io emission labelled. Arrows indicate Io decametric emission and non-Io decametric  
 398 emissions and also solar emissions.

390 and 23:30, this may be the same radio source on active field lines seen at 10:00 sub-corotating  
 391 back into view.

399 Figure 2 shows the timing of these radio emissions relative to the X-ray and UV  
 400 emissions and solar wind conditions. This shows that all the non-Io decametric arcs de-  
 401 tected during the HST campaign were contemporaneous with UV main and polar auroral  
 402 brightening. Most detected arcs appear to occur within 2 days of forward or re-  
 403 verse solar wind shocks, with the possible exceptions of the arcs on 13-14 February and  
 404 10 March, for which there were not clear solar wind shocks.

405 The vertex early and late decametric arc morphology observed on March 10th oc-  
 406 curred within the same Jupiter rotation as the brightest UV main emission of the cam-  
 407 paign (power  $\sim 2$ -4 TW) and during an increase in brightness of the polar emissions by  
 408 a factor of 4 (up to  $\sim 2$  TW). The observation on March 10 was abnormally bright and  
 409 exhibited auroral morphology which may fit one of three different criteria outlined by  
 410 *Grodent et al.* [2018]. The dawn storm feature has a morphology most like an injection  
 411 event auroral morphology. These typically develop over timescales of a Jupiter rotation  
 412 and can be internally driven. Given that solar wind propagations were not suitable at  
 413 this time due to the large Earth-Sun-Jupiter angle, we also explored the SOHO-LASCO  
 414 ICME catalogues to test whether a radially moving ICME may not have appeared in the  
 415 solar wind propagations. Unfortunately, we were unable to draw a firm conclusion as to  
 416 whether this significant brightening of the UV aurora and these early and late vertex non-  
 417 Io arcs were internally or externally driven. For further details see the supporting infor-  
 418 mation.

Date	$\chi^2$ of fit	kT (keV)	CX Flux (ph/cm <sup>2</sup> /s)	S:O	Bremsstrahlung
24-25th Feb S+O	0.85	0.19±0.01	2.0±0.1 x 10 <sup>-6</sup>	0.8	Yes
3rd March S+O	1.1	0.26±0.05	7±3 x 10 <sup>-7</sup>	0.9	No
7th March S+O	0.89	0.11±0.04	7±3 x 10 <sup>-6</sup>	0.6	No
8-9th March S+O	1.3	0.25±0.04	1±1 x 10 <sup>-6</sup>	1.24	No
24-25th Feb SW	1.16	0.22±0.01	2.0±0.2 x 10 <sup>-7</sup>	N/A	Yes
3rd March SW	1.1	0.23±0.02	1.7±0.2 x 10 <sup>-7</sup>	N/A	No
7th March SW	1.2	0.19±0.02	1.1±0.3 x 10 <sup>-7</sup>	N/A	No
8-9th March SW	1.0	0.19±0.01	4.6±0.5 x 10 <sup>-7</sup>	N/A	No

440 **Table 3.** Best-fit Parameters for Iogenic (S+O) and solar wind (SW) atomic charge exchange  
441 (CX) model fits to the XMM-Newton EPIC-pn Northern Auroral Spectra. This shows for each  
442 observation: the  $\chi^2$  of the best fit model, the temperature of the ion distribution, the photon  
443 fluxes produced from ion charge exchange, the ratio of S:O, and whether a Bremsstrahlung con-  
444 tinuum improved the fit. We note that the temperature of the distribution is not built to reflect  
445 the complexity of the collision of ions with Jupiter’s atmosphere, but provides a useful qualitative  
446 diagnostic of the energisation of the population during different intervals (see *Dunn et al.* [in  
447 review] for details).

## 419 6 X-ray Observation Analysis

### 420 6.1 Interpreting the Conditions During Each X-ray Observation

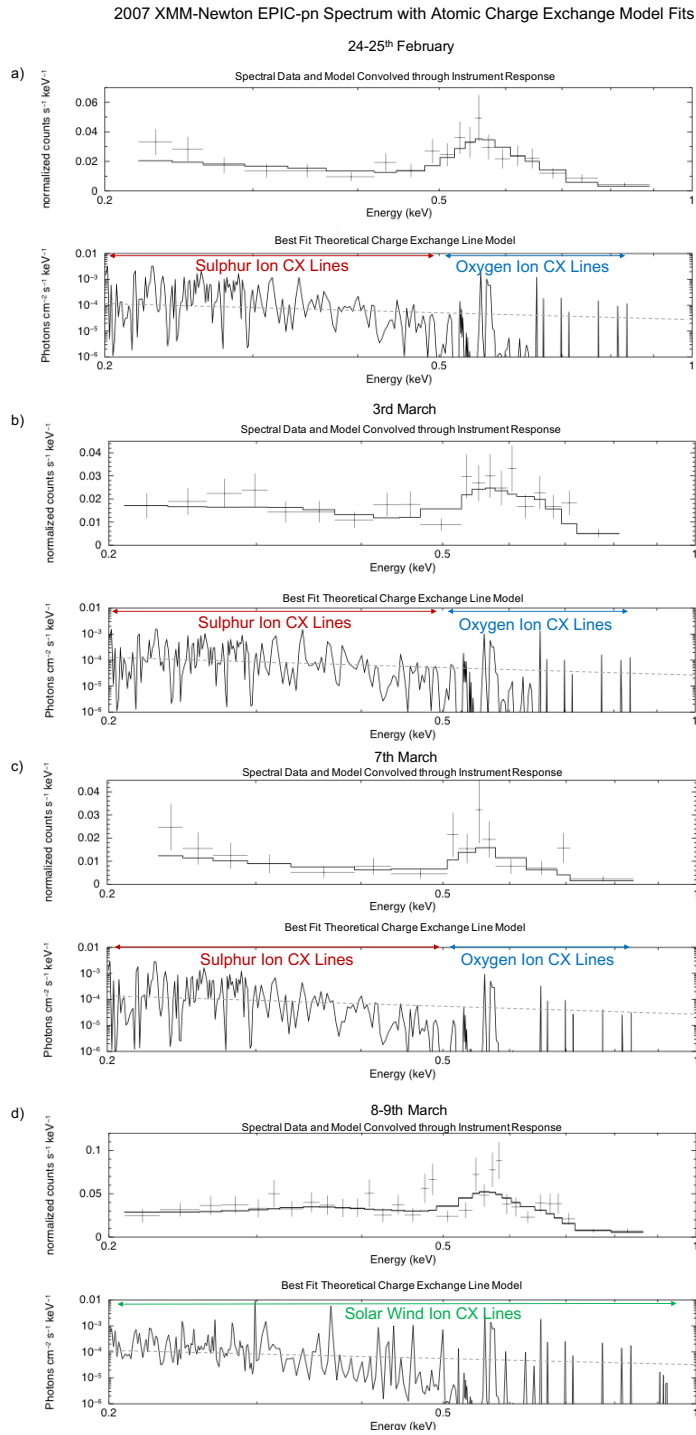
421 The observation on February 8th occurs during the second compression of the mag-  
422 netosphere within a few days, while Feb 10-11th occurs when the magnetosphere has ex-  
423 panded back to  $\sim 100 R_J$ . February 24-25th is the peak of solar wind compression D2-  
424 E2-F2 with a magnetopause stand-off distance of  $\sim 50 R_J$ . It may be that the 8th Feb  
425 observation is dimmer than 24-25th Feb because, as found by *Kita et al.* [2016], the mag-  
426 netosphere had already been in a compressed state very recently. March 3rd is either at  
427 the end of a prolonged period of stable rarefied slow solar wind or at the start of a so-  
428 lar wind compression from CIR A3-B3-C3. Conditions on March 7th and 8-9th seem to  
429 occur when the magnetosphere is expanding back to  $\sim 100 R_J$  following a prolonged in-  
430 terval of compression.

### 431 6.2 X-ray Spectra

432 In the companion paper to this [*Dunn et al.*, in review], we introduce the method  
433 for fitting Jupiter’s X-ray auroral spectra with atomic charge exchange spectral line lists  
434 from AtomDB (<http://www.atomdb.org/> - *Smith et al.* [2012]) and contrast fits for Chan-  
435 dra ACIS with XMM-Newton EPIC spectra. That analysis showed that Chandra ACIS  
436 appears to systematically under-report Jovian auroral emission between 0.45-0.6 keV,  
437 which is key for studies of the oxygen emission in the spectrum. Here, we therefore fo-  
438 cus on the XMM-Newton EPIC-pn spectra and follow the spectral extraction and fit-  
439 ting methods outlined in the companion paper.

458 Figure 5 shows the best fit models and spectra for each observation, while Table  
459 3 shows their best fit parameters. Feb 24-25th was the only observation where adding  
460 a bremsstrahlung continuum provided a better fit. This supports the low hard X-ray counts  
461 recorded by Chandra (Figure 2a) and suggests that bright hard X-ray emission may not  
462 be common and may be triggered by solar wind compressions.

463 For each observation, we compared charge exchange spectrum models for a precip-  
464 itating iogenic ion population (sulphur+oxygen), suggesting a magnetospheric source for



448 **Figure 5.** XMM-Newton EPIC-pn Northern Aurora spectral data from 2007 with their re-  
 449 spective best-fit charge exchange models for a) February 24-25th, b) March 3rd, c) March 7th,  
 450 d) March 8-9th. Upper panels respectively are the best fit atomic charge exchange spectral mod-  
 451 els convolved through the instrument response (black line) and plotted with the XMM-Newton  
 452 EPIC-pn observation (crosses). Lower panels respectively show the best fit theoretical atomic  
 453 charge exchange models of iogenic ions (sulphur+oxygen) or a solar wind ion population (compo-  
 454 sition based on in-situ measurements in *Von Steiger et al. [2000]*), with bremsstrahlung contin-  
 455 uum where this provided an improved fit. The dashed line on charge exchange models illustrates  
 456 the cut-off for spectral lines expected to produce a signature at greater than 0.01 normalised  
 457 counts per s per keV.

465 the precipitating ions, with a solar wind ion population (using the ion abundances in *Von Steiger*  
 466 *et al.* [2000]). We found that for 24-25th Feb and 7th March, an iogenic ion population  
 467 provided a better fit to the data (Table 3). Figure 5 shows that the March 8-9th spec-  
 468 trum is clearly morphologically quite different from the 24-25th Feb and 7th March spec-  
 469 tra. The rising rather than falling emission from 0.2-0.35 keV and emissions between 0.4-  
 470 0.5 keV were better fitted by a solar wind ion population, than a purely sulphur and oxy-  
 471 gen population, suggesting that solar wind ions precipitated in Jupiter’s polar region at  
 472 this time. The 3rd of March spectrum shares morphological features with both an io-  
 473 genic population and solar wind population and both models were able to produce an  
 474 equally good fit to the spectrum.

### 475 6.3 Auroral Morphology

498 The spatial, spectral and temporal resolution of Chandra ACIS allowed us to re-  
 499 register the X-rays photons to their Jovian System III (S3) latitude-longitude positions  
 500 so that the different spatial distributions of the aurora could be explored. At latitudes  
 501 equatorward of the auroral zone there are sparsely distributed X-ray emissions from so-  
 502 lar X-ray photons scattered in Jupiter’s atmosphere. Figure 6 shows that while the X-  
 503 ray aurora is always dominantly poleward of the UV main emission (as defined by con-  
 504 tours mapping to 15 and 45  $R_J$  [*Vogt et al.*, 2015]) , the X-ray aurora morphology does  
 505 vary. For the observations when the magnetosphere is compressed (e.g. Feb 8th and 24-  
 506 25th) the X-ray aurora is concentrated into a localised bright region within longitudes  
 507 up to  $180^\circ$ , while for the expanded magnetosphere cases it is more patchy and extended  
 508 across the polar region (e.g. Feb 10-11th and March 8-9th). Feb 8th and Feb 10-11th  
 509 observations have almost identical CML coverage showing that this changing spatial ex-  
 510 tent is not due to different visibility. These differences may suggest a link between the  
 511 X-ray morphology and the magnetosphere size or solar wind conditions.

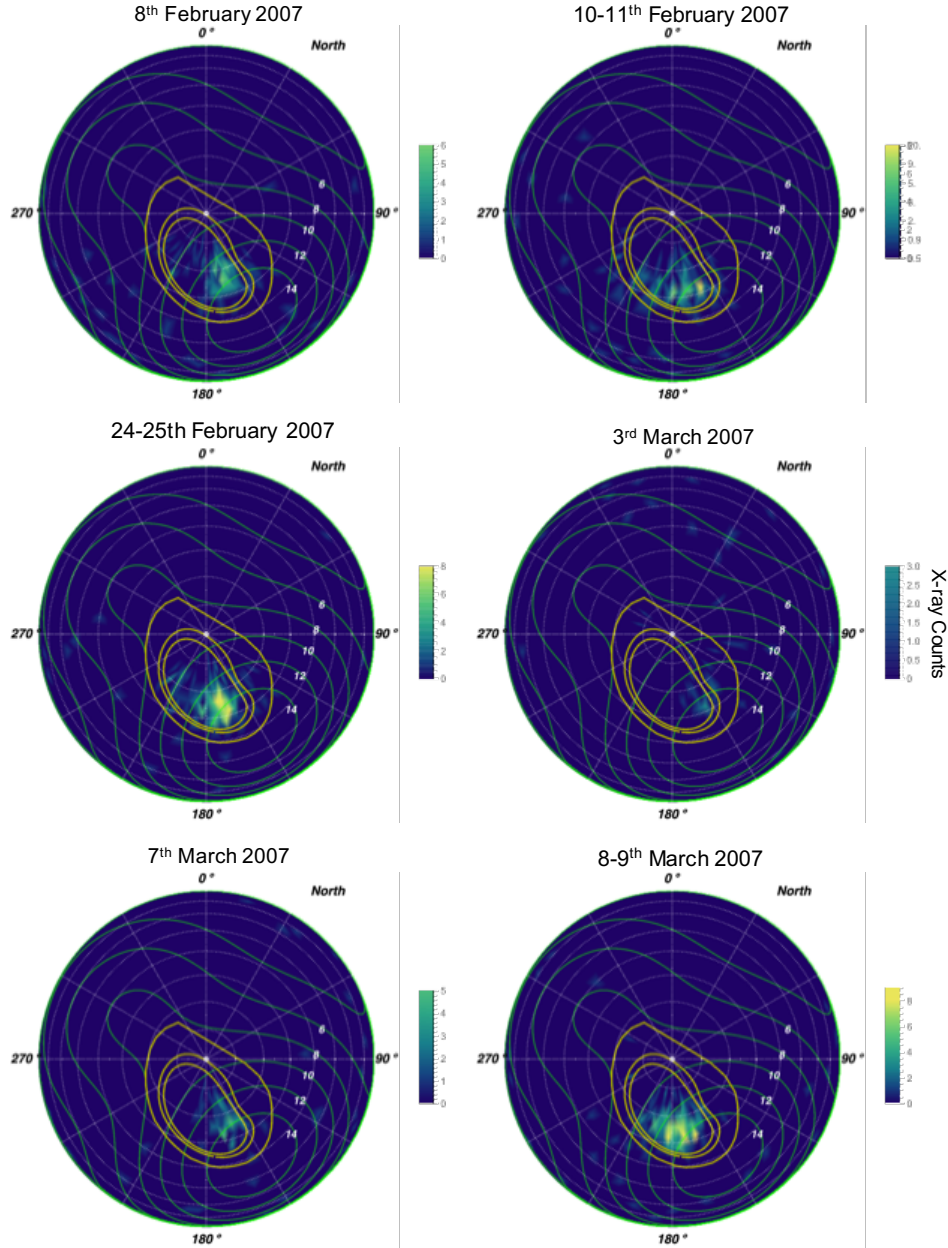
512 Polar projections for the ion energy bands of 0.2-0.5 keV (sulphur/carbon emission)  
 513 and 0.5-0.9 keV (oxygen emission) (Figures 7 and 8) suggest that oxygen emission is typ-  
 514 ically more localised, while sulphur emission is more broadly distributed. As discussed  
 515 by *Dunn et al.* [2016], sulphur requires less energy to generate X-rays so this may demon-  
 516 strate differing distributions of potential drops across the pole.

517 Figure 9 contrasts the X-ray electron bremsstrahlung spatial distribution with the  
 518 distribution from ion lines (0.2-0.5 keV). There are only two observations with a signif-  
 519 icant hard X-ray signal. For 10-11th Feb, the emission is very dim and along the expected  
 520 location of the UV main emission. For 24-25th Feb, in the dawn sector the hard X-rays  
 521 are along the expected main emission location, but in the dusk sector they are shifted  
 522 poleward of this. The UV main emission was particularly bright (power of  $\sim 1$  TW, see  
 523 Fig 2) during this interval and was also shifted polewards in the dusk sector (Fig. 3) such  
 524 that the hard X-rays are still co-located with the UV main emission location. For the  
 525 other X-ray observations, the UV main emission power was around 500 GW and the hard  
 526 X-ray emission appears to be very low ( $\sim 1$  count per hour for Chandra ACIS).

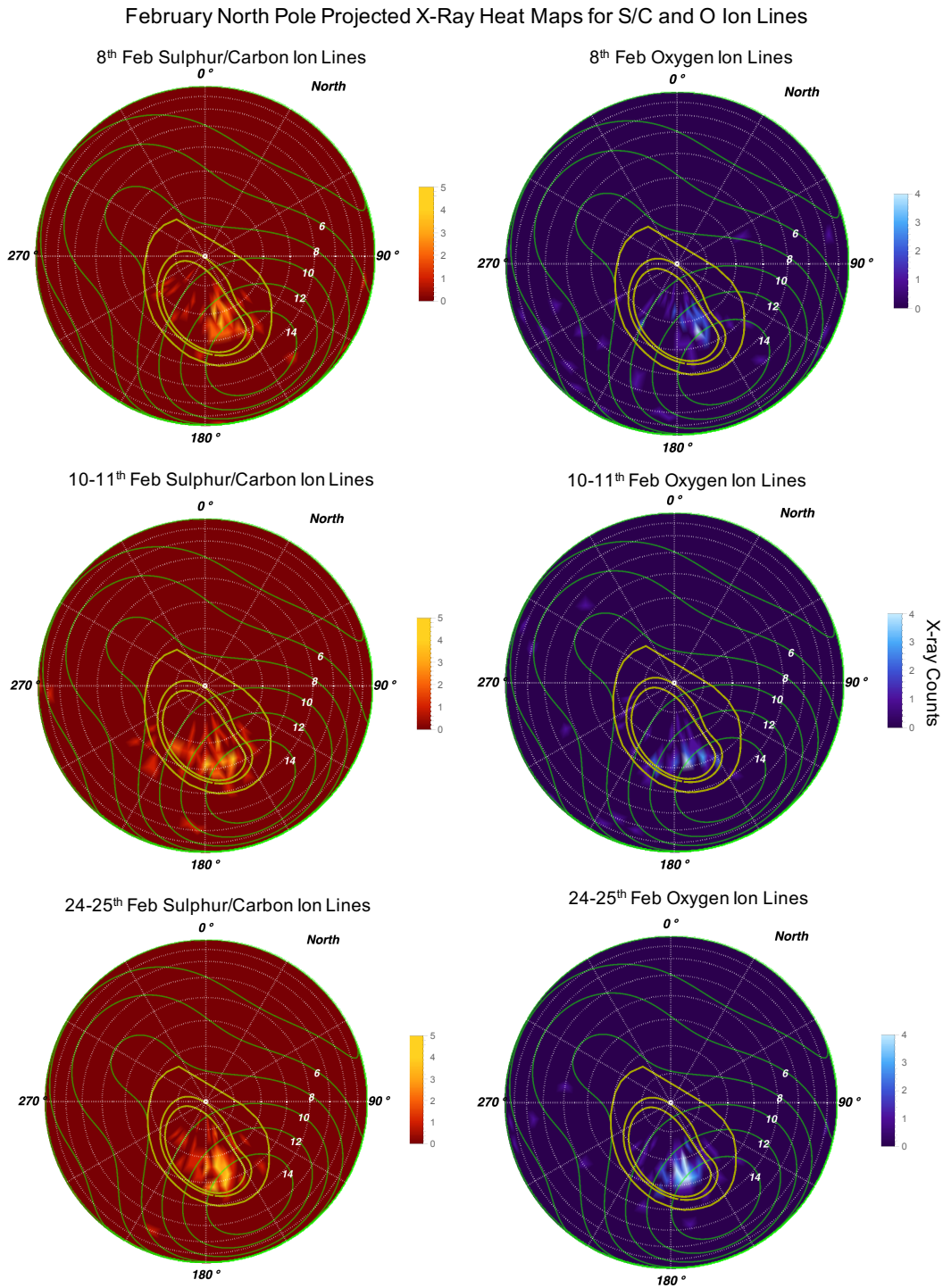
527 The 24-25th Feb hard X-rays also seem co-located with soft X-rays from precip-  
 528 itating ions. It could be that this region produces high energy electron and ion precip-  
 529 itation or that they are so closely located that Chandra’s spatial resolution would not  
 530 resolve their separation. Figure 9 also hints at some possible emission on the 10-11th of  
 531 February close to Io’s footprint at around  $240^\circ$  S3 longitude. Here, the surface magnetic  
 532 field strength decreases which would allow drifting and/or bouncing particles to more  
 533 easily access the atmosphere, since the mirror point would be closer to the atmosphere.  
 534 However, we note that these photons were emitted close to the observed limb of the planet  
 535 and therefore the obliquity of the viewing angle may mean that the emission is projected  
 536 closer to the Io footprint than its true origin location. Establishing whether these pho-



## North Pole Projected X-Ray Heat Maps Observation-to-Observation



476 **Figure 6.** Chandra ACIS projected X-ray Heat maps centred on Jupiter's North pole, showing  
 477 the 0.2-5 keV energy range of emission. The logarithmic color bar indicates the number of  
 478 X-rays in bins of  $3^\circ$  by  $3^\circ$  of S3 latitude-longitude. All projections are scaled to saturate the  
 479 color bar at 8 counts. Dashed grey lines of longitude radiate from the pole, increasing clockwise  
 480 in increments of  $30^\circ$  from  $0^\circ$  at the top. Concentric grey circles outward from the pole represent  
 481 lines of latitude in increments of  $10^\circ$ . Thin green contours with white text labels indicate the  
 482 VIP4 [Connerney *et al.*, 1998] model magnetic field strength in Gauss. Thick gold contours show  
 483 the magnetic field ionospheric footprints of field lines intersecting the Jovigraphic equator at  $5.9$   
 484  $R_J$  (Io's orbit),  $15 R_J$  and  $45 R_J$  [Grodent *et al.*, 2008; Vogt *et al.*, 2015] from equator to pole  
 485 respectively.

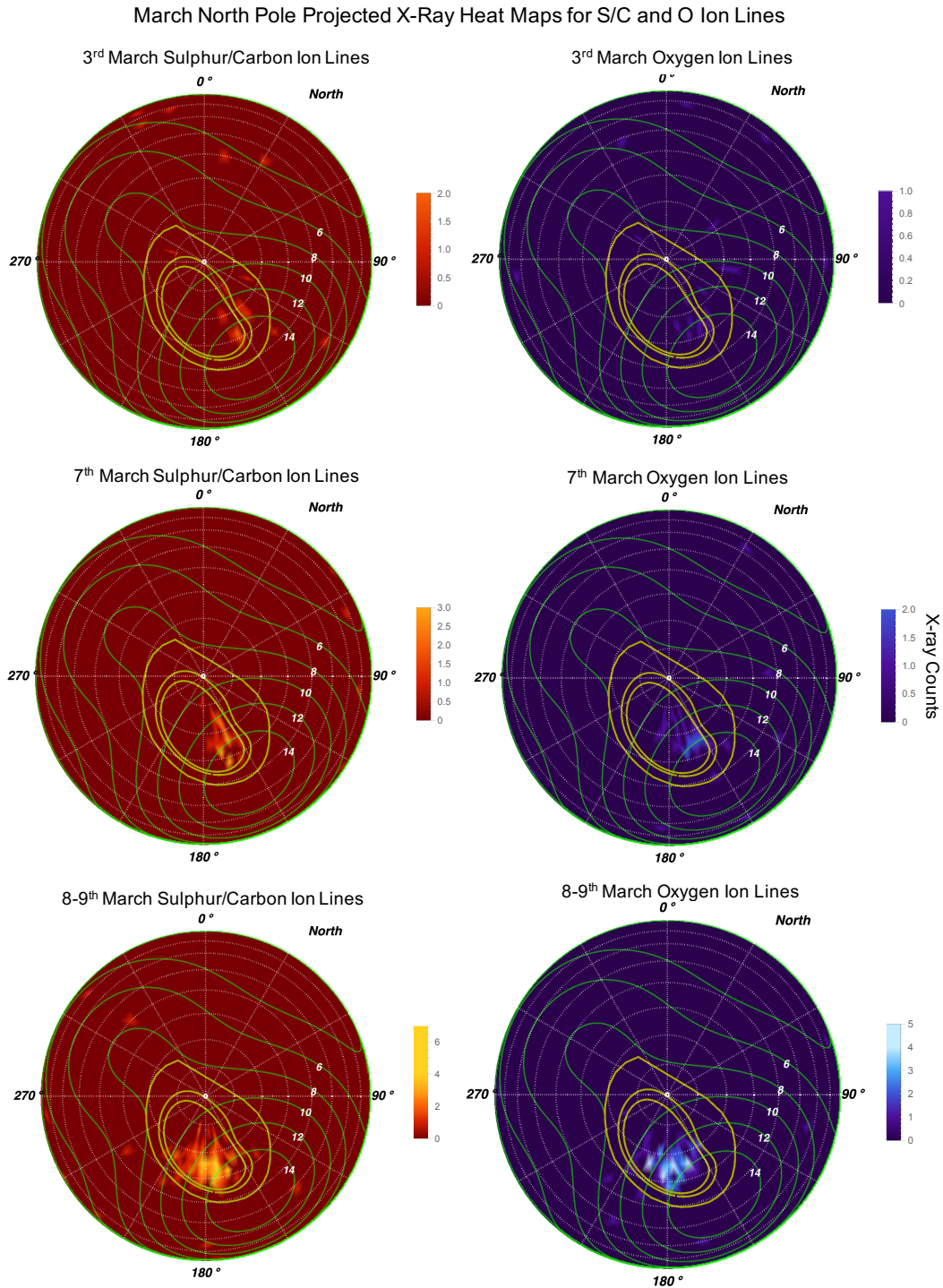


486 **Figure 7.** Projected density maps centred on Jupiter's North pole from Chandra ACIS, comparing the 200-500eV emission from sulphur/carbon ions (left) with the 500-900 eV emission from oxygen ions (right) for the February 2007 observations, with both scaled to saturate the color bar at 5 counts. For further details see Fig. 6.

487

488

489

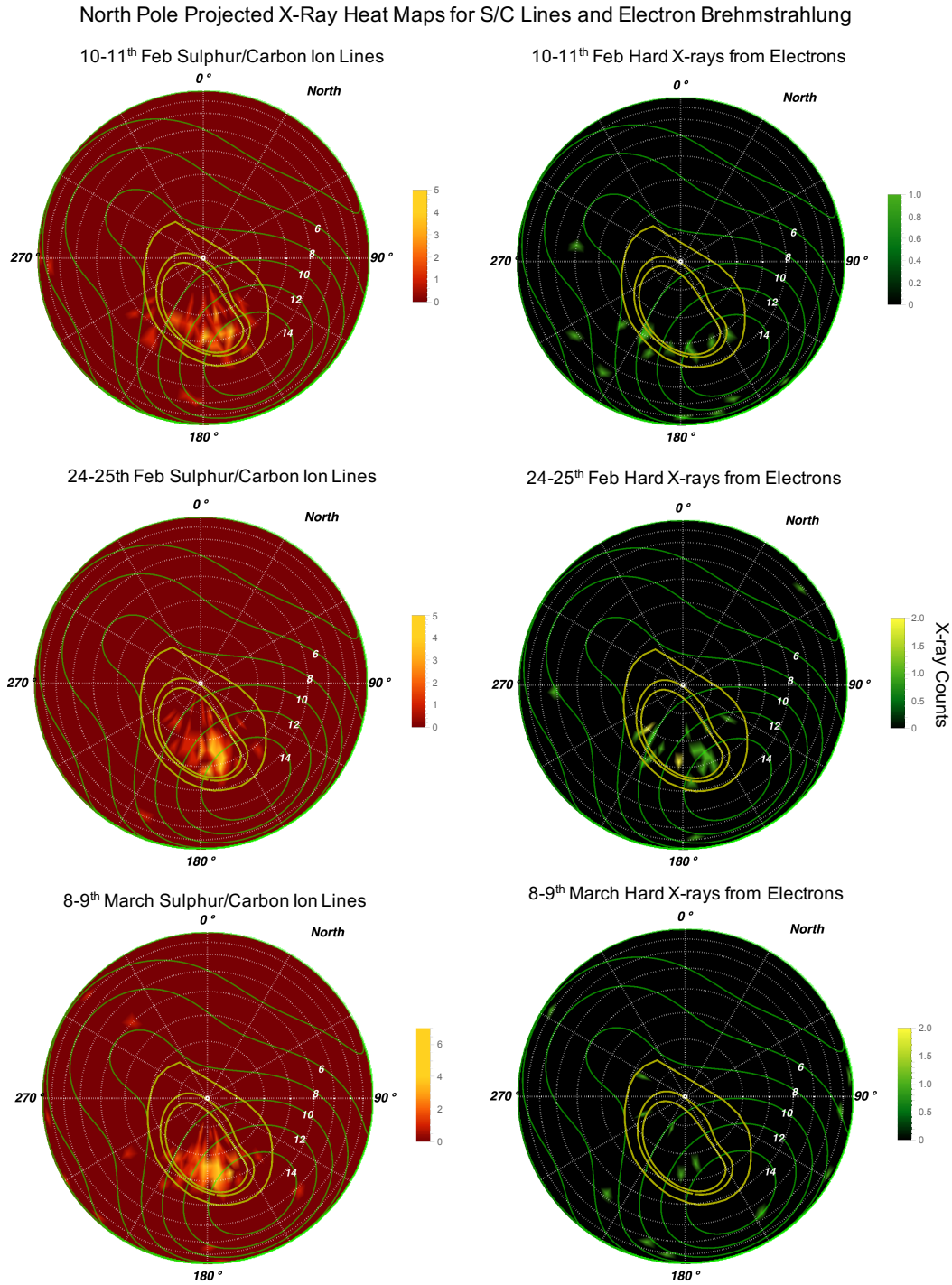


490 **Figure 8.** Projected density maps centred on Jupiter’s North pole from Chandra ACIS, comparing the 200-500eV emission from sulphur/carbon ions (left) with the 500-900 eV emission from oxygen ions (right) for the March 2007 observations, with both scaled to saturate the color bar at 5 counts. For further details see Fig. 6.

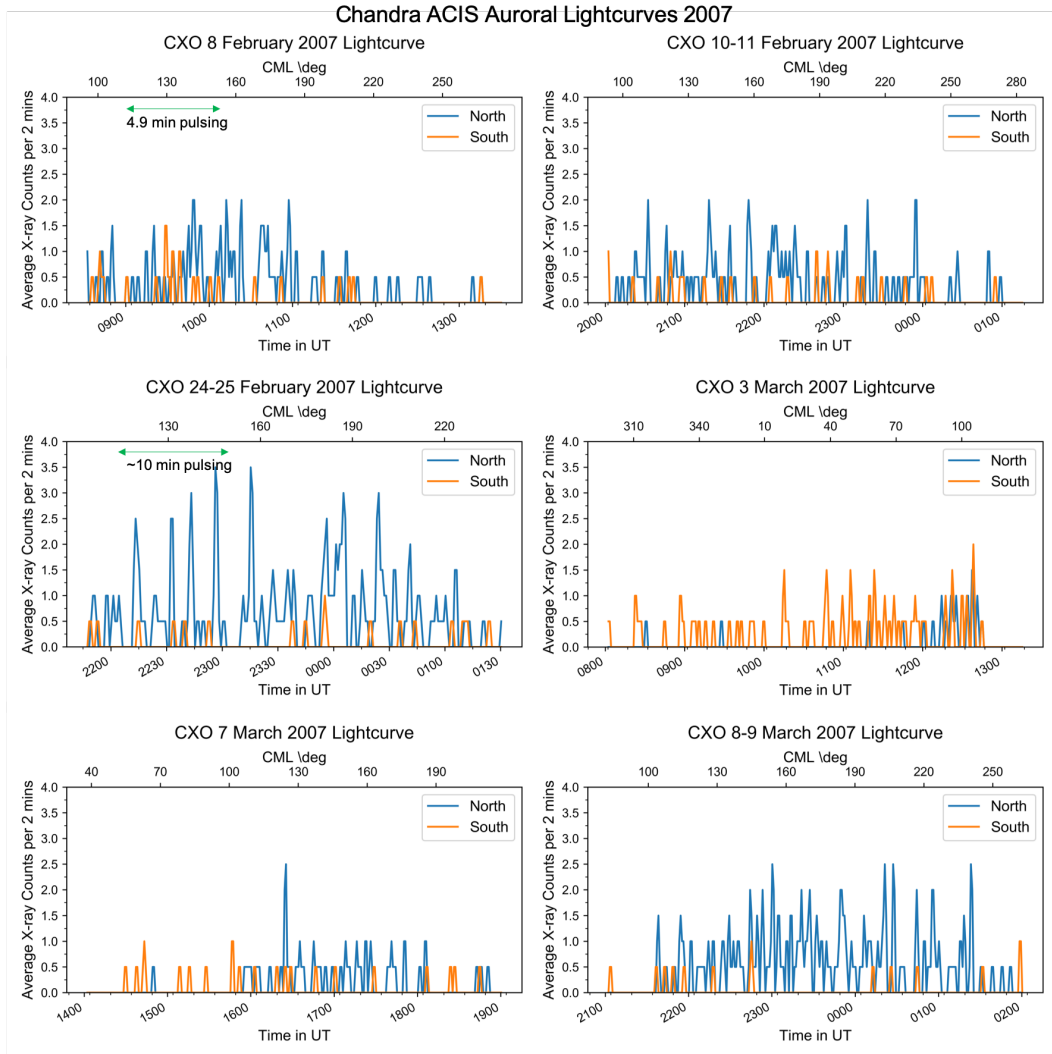
491

492

493



494 **Figure 9.** Projected density maps centred on Jupiter’s North pole from Chandra ACIS,  
 495 comparing the 200-500eV emission from sulphur/carbon ions (left) with the greater than 1 keV  
 496 emission from electrons for observations on the 8th Feb (top), 24-25th Feb (middle) and 8-9th  
 497 March (bottom) 2007. For further details see Fig. 6.



545 **Figure 10.** Chandra ACIS X-ray lightcurves from the Northern (blue) and Southern (gold)  
 546 aurora for each observation. Central Meridian Longitude is indicated across the top, while time  
 547 is along the bottom of the x-axis. The lightcurves are 1-minute binned, with 2-minute moving-  
 548 average smoothing. The green horizontal arrows show intervals when Power Spectral Density  
 549 plots (Figure 13) shows hints of regular pulsations.

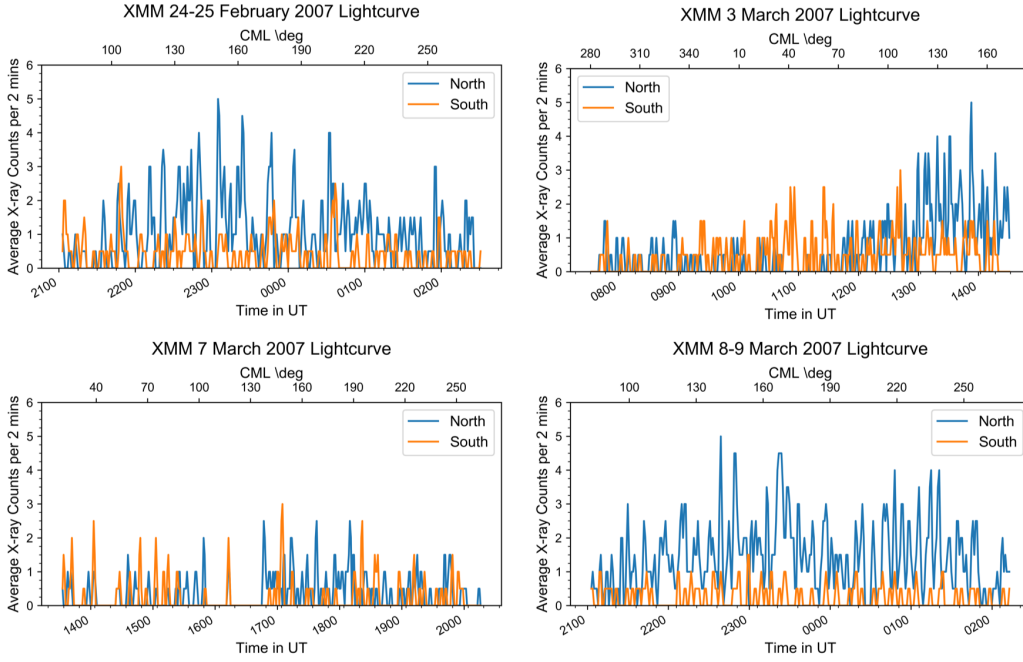
537 tons are indeed from the Io flux tube or Io Plasma Torus will therefore require additional  
 538 exploration with observations with a more favourable viewing geometry.

#### 539 6.4 Timing Signatures

540 We present Chandra and XMM-Newton auroral lightcurves, but expect differences  
 541 because of each instrument's energy-dependent responses and because Chandra's higher  
 542 spatial resolution permitted lightcurve extraction from S3 coordinates centred on the au-  
 543 rora (extracted above  $55^\circ$  latitude), while XMM-Newton's lower spatial resolution meant  
 544 all emission from the Northern or Southern polar region was used.

572 The Northern aurora lightcurves reveal changing behaviour from observation to ob-  
 573 servation (Figures 10 & 11). By examining how X-ray counts are distributed across time

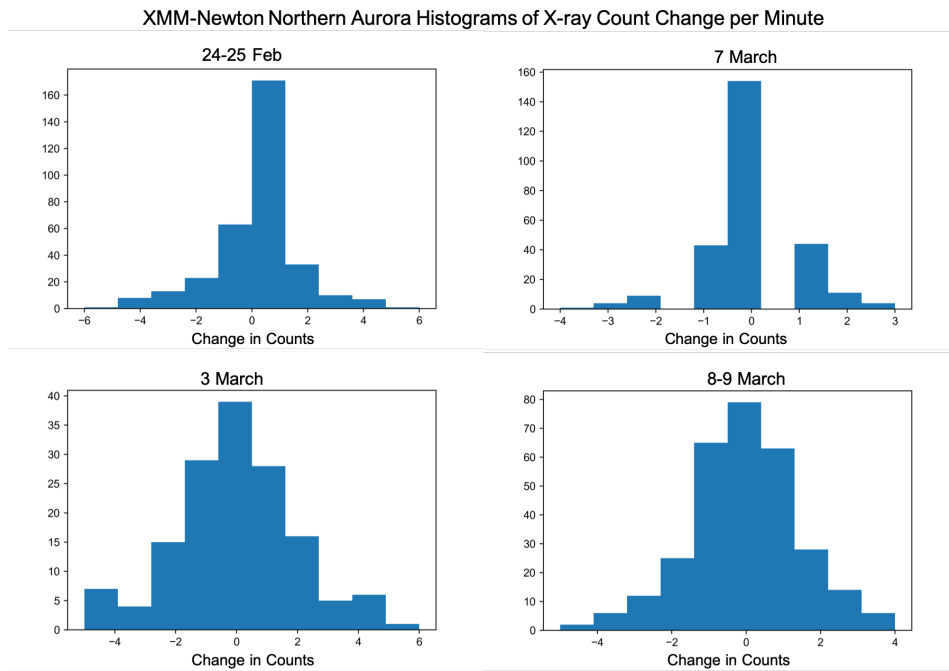
## XMM-Newton EPIC-pn Auroral Lightcurves 2007



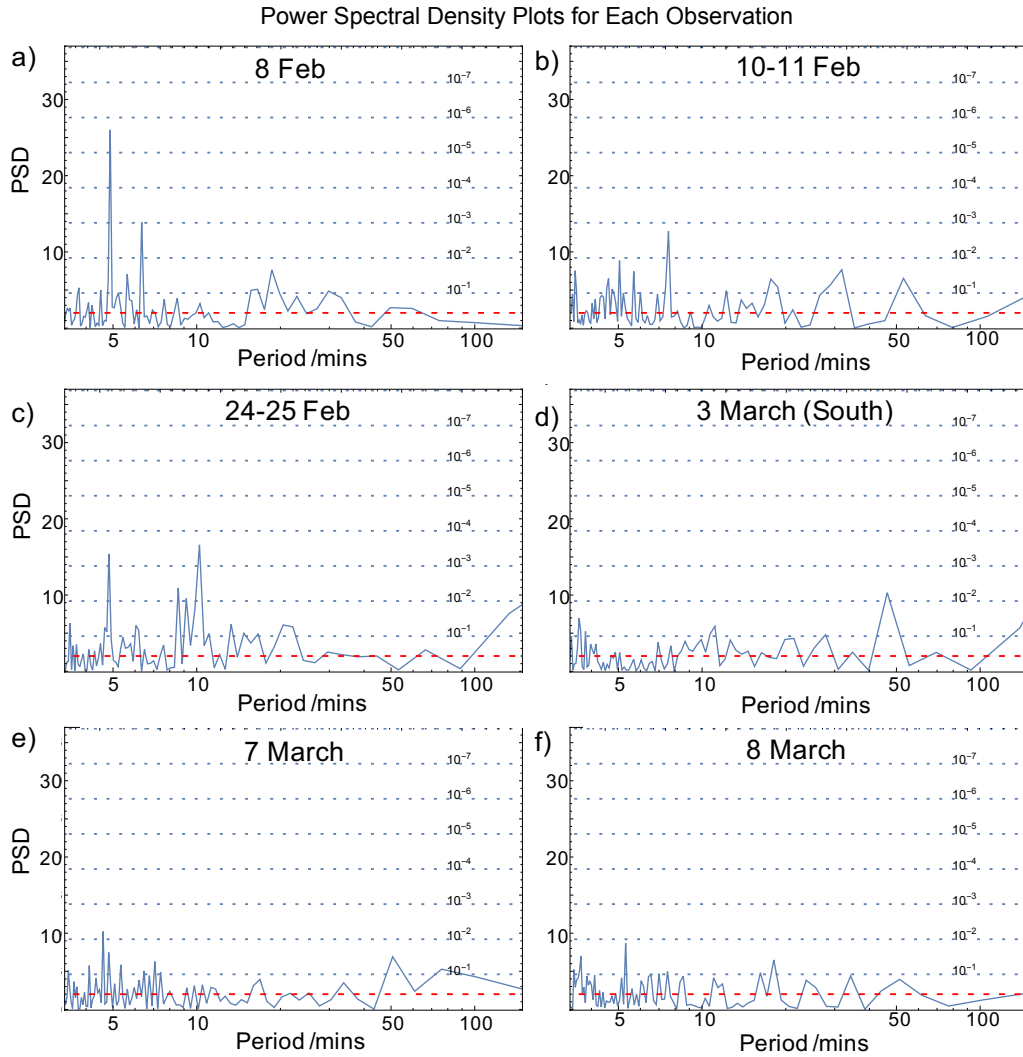
550 **Figure 11.** XMM-Newton EPIC-pn X-ray lightcurves from the Northern (blue) and South-  
 551 ern (gold) aurora for each observation. Central Meridian Longitude is indicated across the top,  
 552 while time is along the bottom of the x-axis. The lightcurves are 1-minute binned, with 2-minute  
 553 moving-average smoothing.

Observation	$\mu$	$\sigma$	$\frac{\sigma}{\mu}$	Temporal Behaviour
CXO 8 Feb	0.3	0.7	2.33	Regular Pulses
CXO 10-11 Feb	0.4	0.7	1.75	Ir/regular Pulses
CXO 24-25 Feb	0.6	1.0	1.67	Regular Pulses
CXO 7 Mar	0.2	0.5	2.5	Irregular Pulses
CXO 8-9 Mar	0.6	0.8	1.33	Flickering+ Irregular Pulses
XMM 24-25 Feb	1.0	1.3	1.3	Regular Pulses
XMM 3 Mar	1.3	1.4	1.08	Flickering + Irregular Pulses
XMM 7 Mar	0.4	0.7	1.75	Irregular Pulses
XMM 8-9 Mar	1.4	1.3	0.93	Flickering + Irregular Pulses

554 **Table 4.** Means ( $\mu$ ), standard deviations ( $\sigma$ ) and coefficients of variation ( $\frac{\sigma}{\mu}$ ) for the number  
 555 of counts per 1 minute bin for the Northern aurora during 2007. The final column summarises  
 556 the temporal behaviour of the X-ray aurorae during each observation as determined from the  
 557 combination of lightcurves, histograms and fast fourier transforms (Figures 10, 11, 12 and 13).



558 **Figure 12.** Histograms of the XMM-Newton Northern aurora showing how the number of  
 559 counts in each 1-minute time bin changes from one time bin to the next. These show two possible  
 560 behaviours in the timing of emission: highly pulsed emission (24-25 Feb and 7 March) vs short  
 561 time interval (1-2 minute) small changes in emission that we define as ‘flickering’ X-ray aurora (3  
 562 March and 8-9 March).



563 **Figure 13.** Power Spectral Density (PSD) plots from fast fourier transforms of the Chandra  
 564 X-ray lightcurves from the X-ray hot spots in 2007, following the normalisation and significance  
 565 methods laid out in *Leahy et al.* [1983] and first applied to Jupiter in *Elsner et al.* [2005]. The  
 566 dashed red lines show the value obtained for poisson statistics applied to a steady source (i.e.  
 567 if the source signal was not pulsed, but still had low counts subject to Poisson statistics). The  
 568 dotted horizontal lines show single-frequency probability chance occurrences (PCO) for the de-  
 569 tected periods. The lowest statistical significant and highest PCO of  $10^{-1}$  is at the bottom of the  
 570 plot. Lightcurves were extracted from  $155\text{-}180^\circ$  longitude and poleward of  $60^\circ$  latitude for the  
 571 Northern hot spot and  $30\text{-}80^\circ$  longitude and poleward of  $-65^\circ$  latitude for the Southern hot spot.



574 bins and through fast fourier transforms (FFTs) of the lightcurves, we identify three types  
 575 of temporal behaviour exhibited by Jupiter’s X-ray aurora during 2007: regular pulsed  
 576 behaviour, irregular pulsed behaviour and ‘flickering’ emission. The pulsed behaviours  
 577 occur when the X-rays are concentrated into short-lived, (1-2 minute duration) impul-  
 578 sive bursts of emission which are bounded by long intervals of dim no emission between  
 579 each burst. Examining the distribution of counts across time bins and the change in counts  
 580 from each time bin to the next shows two statistical characteristics of pulsed behaviour:  
 581 the distribution of the change in counts per time bin is highly peaked (Figure 12) and  
 582 consequently the coefficient of variation (the standard deviation divided by the mean)  
 583 is larger for pulsed intervals (Table 4), for each respective instrument.

584 Power Spectral Density (PSD) analysis, such as that produced by FFTs, confirms  
 585 whether pulses occur regularly or not (Figure 13). The 8th, 10-11th, 24-25th February,  
 586 and the 7th March all exhibited pulsed behaviour. The 8th of February has regular in-  
 587 tervals of  $\sim 5$  minutes between each pulse from 09:00 to 10:30 UT, and the 24-25 Febru-  
 588 ary appears to have  $\sim 10$  minute periodicity from 22:00-23:00, although this is less sta-  
 589 tistically significant in the FFTs. *Jackman et al.* [2018] also reported a regular 4.9 minute  
 590 pulsation period with a 96% confidence for the 8th Feb observation, but this included  
 591 the entire time window and was not filtered by system III coordinates, as the PSDs shown  
 592 here are. For the pulsed behaviour on 10-11th Feb and 7th March, the PSDs do not show  
 593 any strong regularity.

594 What we define as ‘flickering’ behaviour can also appear to be steady emission if  
 595 the time bins of the aurora are larger than 1-minute or if it is smoothed as shown in Fig-  
 596 ures 10 & 11. This behaviour is a short-timescale (1-2 minute) variable dim (not as bright  
 597 as pulses) emission of photons, which is continuous for several hours (i.e. does not have  
 598 prolonged intervals without emission). Flickering behaviour is characterised by a broader  
 599 structure for the distribution of changing counts per bin (Figure 12) and smaller coef-  
 600 ficients of variation (Table 4), for each respective instrument. Inspection of the North-  
 601 ern aurora XMM lightcurves for the 3rd and 8-9th March, shows these ‘flickering’ or steady  
 602 emissions, superposed with pulsed emissions. For example, the 8-9th March has com-  
 603 parably bright flares to 24-25 Feb, but the interval between these bright flares is pop-  
 604 ulated by this flickering or steady emission. There are also intervals of heightened con-  
 605 tinuous X-ray emission, such as that between 23:15-23:30 on 8-9th March, when XMM  
 606 continuously detects 3-5 X-rays every minute from the aurora. This 15 minute interval  
 607 produces almost as much auroral X-ray emission as the entire 7th March observation.  
 608 A similar prolonged bright enhancement was also observed in 2011 [*Dunn et al.*, 2016].  
 609 While the short duration (approx. 1 min) pulses are sometimes co-located with UV flares  
 610 [*Elsner et al.*, 2005], neither the X-ray ‘flickering’ nor the structure that lasts  $\sim 15$  min-  
 611 utes have yet been connected to UV emissions.

## 612 7 Summary of Results and Discussion

613 The combination of the solar wind measurements and radio emissions suggest that  
 614 corotating interaction regions compressed Jupiter’s magnetosphere between the 4th-5th  
 615 February, 22nd-23rd of February and 3rd-4th of March 2007. The magnetosphere then  
 616 expanded back to an uncompressed state between the 9th-10th February, 26th of Febru-  
 617 ary and 7th-10th March respectively. The UV aurora clearly evolves in phase with these  
 618 compressions, as catalogued here and in *Nichols et al.* [2009b] and *Grodent et al.* [2018].  
 619 The majority of the detected non-Io Decametric emissions also appear to be well-aligned  
 620 with solar wind shocks and occur contemporaneously with UV polar and main emission  
 621 auroral brightening. Any connection between the non-Io decametric emissions and X-  
 622 ray aurorae is less evident.

623

## 7.1 X-ray Trends with Solar Wind Conditions

624

625

626

627

628

629

630

631

632

633

634

635

636

637

638

639

These observations presented a rare opportunity to compare Jovian auroral emissions with a measurement of solar wind conditions just upstream of Jupiter. In contrast with previous work using propagation models, we did not find a correlation between solar wind velocity and X-ray emissions. The emissions were brightest during the lowest solar wind velocity and dimmest during faster solar wind, although the velocity difference was small ( $\sim 50$  km/s - Fig. 2). Clearly though, as with the UV aurora, Jupiter's X-ray aurora can be modulated by solar wind shocks; the observation on 24-25th February is affected by a solar wind shock and *Dunn et al.* [2016] also show evidence for shock-driven enhancements. However, the brightest observation of the 2007 campaign (8-9th of March) occurs during modest solar wind velocities and low densities, and when the UV aurora does not exhibit compression morphology, suggesting an expanding/expanded magnetosphere. The very bright 8-9th March observation may suggest that either a) the Interplanetary Magnetic Field direction is critical to producing these additional signatures (it was unmeasured for this campaign), or b) that internal magnetospheric variations and/or processes during expansion are also able to modulate the X-ray aurora behaviour. Here, we attempt to collect and categorise the behaviours observed.

640

## 7.2 Forward Shock Driven X-ray Aurora

641

642

643

644

645

646

647

648

The solar wind forward shock that compressed the magnetopause on 24-25th February appeared to trigger the only bright electron bremsstrahlung emission from the campaign. These emissions were coincident with shifted and expanded UV aurora main emission. Relativistic  $\sim 100$ s keV electrons may be required to produce observable hard X-rays and these may only be present with sufficient fluxes when the UV main emission has powers greater than 1 TW. These electrons would be expected to produce larger current densities and kinetic energy fluxes than their non-relativistic counterparts [*Cowley*, 2006].

649

650

651

652

653

654

655

656

657

658

659

660

661

662

663

Given the excellent fits for a sulphur + oxygen ion population to the spectra, the X-ray pulses during compressions appear to be produced by magnetospheric plasma. This further suggests that the UV active region is also produced by processes inside the outer magnetosphere [e.g. *Bonfond et al.* [2017]]. Under compression, these ion-produced flares occur closer to the electron bremsstrahlung emissions and to a bright pulsing dusk arc of UV emission. *Mauk et al.* [2017] use Juno JEDI data to show that electrons and ions can precipitate together in this region. The quasi-co-location of the electron and ion emissions may be because the outer magnetosphere processes are more spatially confined to a smaller region by the compression. Theoretical studies have also suggested that coupling currents may reverse during solar wind compression [*Cowley and Bunce*, 2003a,b; *Cowley et al.*, 2007; *Yates et al.*, 2014]. If the X-rays do indeed represent the downward currents, then these observations suggest that upward and downward current systems occur closer together and are possibly interspersed during compressions (e.g. *Mauk and Saur* [2007] and *Forsyth et al.* [2014]) (although, X-rays only trace the most energetic ions, so this may not reflect the full extent of the downward current).

664

665

666

667

668

669

670

671

672

673

During magnetospheric compression, the X-ray aurora appears to be more localised, during expansion the emission spreads polewards and longitudinally and is more patchy. This may delineate the halo/core structures that were identified by *Kimura et al.* [2016]. It may be easier to generate a detectable regular periodic pulsation from a compressed magnetosphere, which would have a smaller dayside magnetosphere and therefore fewer processes occurring which could be superposed into the X-ray lightcurve. This would be consistent with the majority of regular X-ray pulsation detections being during intervals of compression [e.g. *Dunn et al.* [2016, 2017]], including those in this paper. Alternatively, *Nichols et al.* [2017a] suggest that UV pulses may be the product of tail reconnection, while *Guo et al.* [2018a,b] suggest that rotation driven reconnection may cause

674 the X-ray aurora. Tail/rotational reconnection would be expected to be enhanced by com-  
 675 pressions of the magnetosphere and to produce pulses of X-ray emission with spectral  
 676 signatures consistent with iogenic plasma, as reported here.

### 677 **7.3 Expanded Magnetosphere or IMF Dependent X-ray Aurora**

678 Arguably the most interesting but puzzling observation of the campaign is March  
 679 8th-9th. It is during an interval of magnetospheric expansion that does not seem to have  
 680 particularly different solar wind velocities or densities than Feb 10-11th or March 7th  
 681 and yet the observation is the brightest in 2007. The spectra suggest that the precip-  
 682 itation of solar wind ions contribute X-ray auroral emissions at this time, while the tim-  
 683 ing signatures suggest that multiple processes produced the X-ray aurora.

684 The X-ray time signatures suggest a combination of bright flares superposed on flick-  
 685 ering emission. If the X-ray emission on the 8-9th March is connected to the UV aurora  
 686 one Jupiter rotation later, then there are two possible counterpart UV emissions on the  
 687 9th March that may explain the steady X-ray emission. The swirl region is dim but ac-  
 688 tive, with low-levels of emission from a few spatial locations, so that this emission may  
 689 appear to ‘flicker’. There is also a rarer long-lasting transpolar filament, which may ex-  
 690 plain the steady polar emission, co-existing with intermittent flares. Polar filaments have  
 691 been suggested to relate to high latitude reconnection [*Nichols et al.*, 2009a] and, if this  
 692 was the case, then they could provide a steady solar wind ion precipitation to generate  
 693 the X-ray spectra observed. However, theoretical arguments show it is difficult to pro-  
 694 duce X-ray aurora through direct solar wind precipitation without bright proton auro-  
 695 ras [*Cravens et al.*, 2003; *Bunce et al.*, 2004]. It may therefore be easier to explain the  
 696 spectral signatures if the outer magnetosphere had a mixed iogenic and solar wind pop-  
 697 ulation. This raises the question of how the solar wind gained entry for this interval, while  
 698 it is not present in the others.

699 It may be that there was an interval of increased reconnection at Jupiter’s mag-  
 700 netopause, which injected solar wind ions into the system through a combination of day-  
 701 side and/or tail reconnection. Alternatively, the mechanical motion of the magnetosphere  
 702 during expansion may permit this solar wind entry. mSWiM propagations with the *Joy*  
 703 *et al.* [2002] model suggest a magnetopause shift from  $\sim 50$  to  $100 R_J$  over the 3 days dur-  
 704 ing which this observation occurs. This expansion would depend on the magnetospheric  
 705 thermal plasma providing sufficient internal pressure following a compression. If the ex-  
 706 pansion of the magnetosphere occurred as a harmonic oscillator this could help trigger  
 707 formation or roll-up of Kelvin Helmholtz Instabilities (KHI), through which solar wind  
 708 ions could enter the magnetosphere [*Ma et al.*, 2017]. Alternatively, during rarefied so-  
 709 lar wind,  $O^{7+}$  ions have a gyroradius of 0.1-0.3  $R_J$  and a gyroperiod of  $\sim 10$ s of minutes  
 710 (assuming velocity of 10% of the bulk and  $B \sim 0.2$  nT, comparable to 10th percentile  
 711 [*Ebert et al.*, 2014; *Bagenal et al.*, 2014]). If the magnetosphere did expand by  $\sim 50 R_J$   
 712 within  $\sim 3$  days, the expansion rate is at a comparable timescale and length-scale to the  
 713 gyroperiod and gyroradii of high charge state ions in the solar wind. It may therefore  
 714 be possible for solar wind ions to simply have gyrated across the magnetopause and into  
 715 the outer magnetosphere.

716 The broader spatial distribution for 8-9th March, could reflect a variety of differ-  
 717 ent possible processes, including reconnection with the solar wind. It could be indica-  
 718 tive of a shift/redistribution of return currents across an extended magnetosphere, which  
 719 may have larger potential drops due to the differing distances and densities. We also pro-  
 720 pose two other possible drivers: as at Earth, magnetospheric expansions can generate  
 721 vortices in the outer magnetosphere. These vortices can produce field aligned current  
 722 systems and associated auroral emissions in locations where they might otherwise not  
 723 exist [*Zhao et al.*, 2016; *Shi et al.*, 2014]. Alternatively, an expanded/ing magnetosphere

724 may enhance radial outward mass transport, which could enhance internal processes such  
725 as reconnection.

726 The limited visibility for the 3rd of March observation combined with the uncer-  
727 tainties on the solar wind conditions, makes it more challenging to fully categorise. How-  
728 ever, it occurs within a few hours of an expanded magnetospheric UV aurora and the  
729 spectrum is equally well fit by iogenic or solar wind ions (without a bremsstrahlung com-  
730 ponent). It also has temporal signatures of pulses and flickering X-ray aurora. The com-  
731 bination of these factors suggest a possible consistency with the 8-9th March observa-  
732 tion or an interval of transition between expanded and compressed states.

#### 733 **7.4 Dim X-ray Aurora During Shock Recovery**

734 10-11th of Feb and 7th of March observations occur during magnetospheric recov-  
735 ery, when the magnetopause is expanding back outwards. They are all very dim due to  
736 a low rate of dim X-ray pulses. Their timing during expansions may help to distinguish  
737 between expansion and IMF-dependent auroral processes for the 8-9th March. Magne-  
738 topause and magnetodisk reconnection, KHI, downward currents and wave interactions  
739 have all been proposed as mechanisms for the X-ray aurora [*Cravens et al.*, 2003; *Bunce*  
740 *et al.*, 2004; *Dunn et al.*, 2017; *Guo et al.*, 2018a; *Manners et al.*, 2018]. These dim ob-  
741 servations may suggest that during shock recovery, conditions are either unfavourable  
742 for whichever process produces the X-ray emissions or that the ion densities/energies are  
743 too low.

## 744 **8 Conclusion**

745 We report trends in the responses of the X-ray, UV and radio emissions of Jupiter  
746 during changing solar wind conditions measured by the New Horizons spacecraft in Febru-  
747 ary and March 2007. A solar wind shock causes the Jovian soft and hard X-ray auro-  
748 rae to brighten on 24-25th Feb. This is the only observation in 2007 with significant hard  
749 X-ray emission and these hard X-rays are co-located with a UV dawn storm and dusk  
750 polar arc, with UV aurora main emission powers of  $\sim 1$  TW. At this time, soft X-ray emis-  
751 sion from ion precipitation, which may indicate the downward currents, is located more  
752 closely to the hard X-rays from the upward current system, than normally observed [e.g.  
753 *Branduardi-Raymont et al.* [2008]], which could suggest a more interspersed upward and  
754 downward current system during magnetospheric compressions. The soft and hard X-  
755 ray emissions appear to be independent and their relative responses can provide impor-  
756 tant clues to the state and dynamics of the magnetosphere. The rarer brightening of the  
757 hard X-ray emission acts as a tracer of solar wind compressions, while the soft X-ray ion  
758 response seems more complex and can also brighten during either magnetospheric ex-  
759 pansions or intervals favourable to reconnection (e.g. 8-9th March).

760 While the polar soft X-ray emissions brighten during both forward shocks and mag-  
761 netospheric expansions, their spectra are very different for the two intervals. Iogenic ion  
762 populations provide a best fit during magnetospheric compressions. For at least one bright  
763 observation with an expanding/ed magnetosphere, the emission has a spectrum that is  
764 best fit by including a population of solar wind ions. The time series data and spatial  
765 distributions of events suggest that superposed on the typical auroral pulses/flares there  
766 is a steady or flickering X-ray source, suggesting multiple processes produce the X-ray  
767 aurora at this time. It also suggests that, while significant abundances of solar wind ions  
768 entering the system is uncommon, that the conditions (IMF direction, rapid magnetopause  
769 expansion and/or harmonic oscillations of the magnetopause) were right for this during  
770 this observation.

771 The 2007 campaign provides a rich multi-waveband observation campaign that demon-  
772 strates that Jupiter's X-ray aurora exhibits several different characteristic behaviours,

773 which coincide with different solar wind and UV auroral conditions. Further observa-  
774 tions will be required to fully constrain the correlations and driving processes for these  
775 intriguing behaviours. The analysis presented here takes important steps towards iden-  
776 tifying these different behaviours and the possible connections with solar wind or inter-  
777 nal drivers.

### 778 **Acknowledgments**

779 W.R.D would like to thank D. McComas for support with the New Horizons SWAP data.  
780 WRD would also like to thank the Vogt/Masters and Jackman/Paranicas ISSI team meet-  
781 ings, which initiated this project. W.R.D. was supported in this work by a Science and  
782 Technology Facilities Council (STFC) research grant to University College London (UCL),  
783 an SAO fellowship to Harvard-Smithsonian Center for Astrophysics and by European  
784 Space Agency (ESA) contract no. 4000120752/17/NL/MH. LL was supported by CNRS/INSU.  
785 CL was funded by CNES. EJB was supported by STFC grant ST/N000749/1 and a Royal  
786 Society Wolfson Research Merit Award. LCR was funded by an STFC consolidated grant  
787 to Lancaster University (ST/R000816/1). C.M.J.'s work at Southampton is supported  
788 by STFC Ernest Rutherford Fellowship ST/L004399/1. C.M.J.'s work at DIAS is sup-  
789 ported by Science Foundation Ireland grant 18/FRL/6199. Z. H. Y. acknowledges finan-  
790 cial support from the Belgian Federal Science Policy Office (BELSPO) via the PRODEX  
791 Programme of ESA. New Horizons SWAP data is available on the NASA Planetary Data  
792 System (PDS): [https://pds-ppi.igpp.ucla.edu/search/?sc=New\\_Horizons&t=Jupiter&i=SWAP](https://pds-ppi.igpp.ucla.edu/search/?sc=New_Horizons&t=Jupiter&i=SWAP).  
793 The authors acknowledge the NDA team (at the Nançay Radio Observatory and LESIA,  
794 Observatoire de Paris) and the Wind/Waves team (at Goddard and LESIA, Observa-  
795 toire de Paris) for providing access to radio data and the ExPRES team (at LESIA, Ob-  
796 servatoire de Paris with support from Paris Astronomical Data Centre) for providing ac-  
797 cess to radio simulations. The NDA data were directly retrieved online at [http://www.obs-](http://www.obs-nancy.fr)  
798 [nancy.fr](http://www.obs-nancy.fr), the ExPRES simulations at <http://maser.obspm.fr/data/expres>, and the Wind/Waves  
799 data from the CDWeb service at <http://cdaweb.gsfc.nasa.gov>. We also greatly thank  
800 the Chandra and XMM-Newton Projects for their support. The Jupiter X-ray observa-  
801 tions presented here are publicly available on the Chandra archive (<https://cda.harvard.edu/chaser/>)  
802 and the XMM-Newton archive (<http://nxsa.esac.esa.int/nxsa-web/#search>) respectively.  
803 The mSWiM solar wind propagation model is publicly available from <http://mswim.engin.umich.edu/>.  
804 Tao model propagated solar wind data are available upon a request to C.T. ([chihiro.tao@nict.go.jp](mailto:chihiro.tao@nict.go.jp))  
805 and publicly available at the AMDA database (<http://amda.cdpp.eu>). The Jupiter UV  
806 observations presented here are publicly available on the ESA Hubble archive: <http://hst.esac.esa.int/ehst>.

## References

- 808 Badman, S., B. Bonfond, M. Fujimoto, R. Gray, Y. Kasaba, S. Kasahara,  
809 T. Kimura, H. Melin, J. D. Nichols, A. Steffl, et al. (2016), Weakening of jupiter’s  
810 main auroral emission during january 2014, *Geophysical Research Letters*, *43*(3),  
811 988–997.
- 812 Badman, S. V., G. Branduardi-Raymont, M. Galand, S. L. Hess, N. Krupp,  
813 L. Lamy, H. Melin, and C. Tao (2015), Auroral processes at the giant planets:  
814 Energy deposition, emission mechanisms, morphology and spectra, *Space Science*  
815 *Reviews*, *187*(1-4), 99–179.
- 816 Bagenal, F., A. Adriani, F. Allegrini, S. Bolton, B. Bonfond, E. Bunce, J. Conner-  
817 ney, S. Cowley, R. Ebert, G. Gladstone, et al. (2014), Magnetospheric science  
818 objectives of the juno mission, *Space Science Reviews*, pp. 1–69.
- 819 Bagenal, F., M. Horányi, D. McComas, R. McNutt, H. Elliott, M. Hill, L. Brown,  
820 P. Delamere, P. Kollmann, S. Krimigis, et al. (2016), Pluto’s interaction with its  
821 space environment: Solar wind, energetic particles, and dust, *Science*, *351*(6279),  
822 aad9045.
- 823 Baron, R., T. Owen, J. Connerney, T. Satoh, and J. Harrington (1996), Solar wind  
824 control of jupiter’s h+ 3 auroras, *Icarus*, *120*(2), 437–442.
- 825 Bhattacharyya, D., J. T. Clarke, J. Montgomery, B. Bonfond, J.-C. Gérard, and  
826 D. Grodent (2018), Evidence for auroral emissions from callisto’s footprint in hst  
827 uv images, *Journal of Geophysical Research: Space Physics*, *123*(1), 364–373.
- 828 Boischoat, A., C. Rosolen, M. Aubier, G. Daigne, F. Genova, Y. Leblanc,  
829 A. Lecacheux, J. de La Noe, et al. (1980), A new high-grain, broadband, steer-  
830 able array to study jovian decametric emission, *Icarus*, *43*(3), 399–407.
- 831 Bonfond, B., D. Grodent, J.-C. Gérard, A. Radioti, V. Dols, P. Delamere, and  
832 J. Clarke (2009), The io uv footprint: Location, inter-spot distances and tail  
833 vertical extent, *Journal of Geophysical Research: Space Physics*, *114*(A7).
- 834 Bonfond, B., M. Vogt, J.-C. Gérard, D. Grodent, A. Radioti, and V. Coumans  
835 (2011), Quasi-periodic polar flares at jupiter: A signature of pulsed dayside recon-  
836 nections?, *Geophysical Research Letters*, *38*(2).
- 837 Bonfond, B., S. Hess, F. Bagenal, J.-C. Gérard, D. Grodent, A. Radioti, J. Gustin,  
838 and J. T. Clarke (2013), The multiple spots of the ganymede auroral footprint,  
839 *Geophysical Research Letters*, *40*(19), 4977–4981.
- 840 Bonfond, B., D. Grodent, S. V. Badman, J.-C. Gérard, and A. Radioti (2016), Dy-  
841 namics of the flares in the active polar region of jupiter, *Geophysical Research*  
842 *Letters*, *43*(23).
- 843 Bonfond, B., G. Gladstone, D. Grodent, T. Greathouse, M. Versteeg, V. Hue,  
844 M. Davis, M. Vogt, J.-C. Gérard, A. Radioti, et al. (2017), Morphology of the  
845 uv aurorae jupiter during juno’s first perijove observations, *Geophysical Research*  
846 *Letters*.
- 847 Bougeret, J.-L., M. L. Kaiser, P. Kellogg, R. Manning, K. Goetz, S. Monson,  
848 N. Monge, L. Friel, C. Meetre, C. Perche, et al. (1995), Waves: The radio and  
849 plasma wave investigation on the wind spacecraft, *Space Science Reviews*, *71*(1-4),  
850 231–263.
- 851 Branduardi-Raymont, G., R. Elsner, G. Gladstone, G. Ramsay, P. Rodriguez, R. So-  
852 ria, and J. Waite Jr (2004), First observation of jupiter by xmm-newton, *Astron-  
853 omy & Astrophysics*, *424*(1), 331–337.
- 854 Branduardi-Raymont, G., A. Bhardwaj, R. Elsner, G. Gladstone, G. Ramsay, P. Ro-  
855 driguez, R. Soria, J. Waite, T. Cravens, et al. (2007), A study of jupiter’s aurorae  
856 with xmm-newton, *Astronomy & Astrophysics*, *463*(2), 761–774.
- 857 Branduardi-Raymont, G., R. F. Elsner, M. Galand, D. Grodent, T. Cravens,  
858 P. Ford, G. Gladstone, and J. Waite (2008), Spectral morphology of the x-ray  
859 emission from jupiter’s aurorae, *Journal of Geophysical Research: Space Physics*

- 860 (1978–2012), 113(A2).
- 861 Bunce, E., S. Cowley, and T. Yeoman (2004), Jovian cusp processes: Implications  
862 for the polar aurora, *Journal of Geophysical Research: Space Physics (1978–2012)*,  
863 109(A9).
- 864 Chané, E., J. Saur, R. Keppens, and S. Poedts (2017), How is the jovian main auro-  
865 ral emission affected by the solar wind?, *Journal of Geophysical Research: Space*  
866 *Physics*, 122(2), 1960–1978.
- 867 Clark, G., B. Mauk, D. Haggerty, C. Paranicas, P. Kollmann, A. Rymer, E. Bunce,  
868 S. Cowley, D. Mitchell, G. Provan, et al. (2017), Energetic particle signatures of  
869 magnetic field-aligned potentials over jupiter’s polar regions, *Geophysical Research*  
870 *Letters*, 44(17), 8703–8711.
- 871 Clarke, J., J. Nichols, J.-C. Gérard, D. Grodent, K. Hansen, W. Kurth, G. Glad-  
872 stone, J. Duval, S. Wannawichian, E. Bunce, et al. (2009), Response of jupiter’s  
873 and saturn’s auroral activity to the solar wind, *Journal of Geophysical Research:*  
874 *Space Physics (1978–2012)*, 114(A5).
- 875 Connerney, J., M. Acuna, N. Ness, and T. Satoh (1998), New models of jupiter’s  
876 magnetic field constrained by the io flux tube footprint, *Journal of Geophysical*  
877 *Research: Space Physics (1978–2012)*, 103(A6), 11,929–11,939.
- 878 Cowley, S. (2006), Current-voltage and kinetic energy flux relations for relativistic  
879 field-aligned acceleration of auroral electrons, in *Annales Geophysicae*, vol. 24, pp.  
880 325–338.
- 881 Cowley, S., and E. Bunce (2001), Origin of the main auroral oval in jupiter’s cou-  
882 pled magnetosphere–ionosphere system, *Planetary and Space Science*, 49(10),  
883 1067–1088.
- 884 Cowley, S., and E. Bunce (2003a), Modulation of jupiter’s main auroral oval emis-  
885 sions by solar wind induced expansions and compressions of the magnetosphere,  
886 *Planetary and Space Science*, 51(1), 57–79.
- 887 Cowley, S., and E. Bunce (2003b), Modulation of jovian middle magnetosphere  
888 currents and auroral precipitation by solar wind-induced compressions and expan-  
889 sions of the magnetosphere: initial response and steady state, *Planetary and Space*  
890 *Science*, 51(1), 31–56.
- 891 Cowley, S., E. Bunce, T. Stallard, and S. Miller (2003), Jupiter’s polar ionospheric  
892 flows: Theoretical interpretation, *Geophysical research letters*, 30(5).
- 893 Cowley, S., J. Nichols, and D. Andrews (2007), Modulation of jupiter’s plasma flow,  
894 polar currents, and auroral precipitation by solar wind-induced compressions and  
895 expansions of the magnetosphere: a simple theoretical model, in *Annales Geophys-*  
896 *icae*, vol. 25, pp. 1433–1463.
- 897 Cowley, S., S. V. Badman, S. Imber, and S. Milan (2008), Comment on jupiter: A  
898 fundamentally different magnetospheric interaction with the solar wind? by dj  
899 mcomas and f. bagenal, *Geophysical Research Letters*, 35(10).
- 900 Cravens, T., E. Howell, J. Waite, and G. Gladstone (1995), Auroral oxygen precip-  
901 itation at jupiter, *Journal of Geophysical Research: Space Physics (1978–2012)*,  
902 100(A9), 17,153–17,161.
- 903 Cravens, T., J. Waite, T. Gombosi, N. Lugaz, G. Gladstone, B. Mauk, and R. Mac-  
904 Dowall (2003), Implications of jovian x-ray emission for magnetosphere-ionosphere  
905 coupling, *Journal of Geophysical Research: Space Physics (1978–2012)*, 108(A12).
- 906 Delamere, P., and F. Bagenal (2010), Solar wind interaction with jupiter’s magneto-  
907 sphere, *Journal of Geophysical Research: Space Physics (1978–2012)*, 115(A10).
- 908 Desch, M., and C. Barrow (1984), Direct evidence for solar wind control of jupiter’s  
909 hectometer-wavelength radio emission, *Journal of Geophysical Research: Space*  
910 *Physics*, 89(A8), 6819–6823.
- 911 Dunn, W., G. Branduardi-Raymont, L. Ray, C. Jackman, R. Kraft, R. Elsner,  
912 I. Rae, Z. Yao, M. Vogt, G. Jones, et al. (2017), The independent pulsations of  
913 jupiter’s northern and southern x-ray auroras, *Nature Astronomy*, 1(11), 758.

- 914 Dunn, W. R., G. Branduardi-Raymont, R. F. Elsner, M. F. Vogt, L. Lamy, P. G.  
 915 Ford, A. J. Coates, G. R. Gladstone, C. M. Jackman, J. D. Nichols, et al. (2016),  
 916 The impact of an icme on the jovian x-ray aurora, *Journal of Geophysical Re-*  
 917 *search: Space Physics*, *121*(3), 2274–2307.
- 918 Dunn, W. R., G. Branduardi-Raymont, V. Carter-Cortez, A. Campbell, R. F.  
 919 Elsner, J.-U. Ness, G. R. Gladstone, P. Ford, Z. Yao, P. Rodriguez, G. Clark,  
 920 C. Paranicas, A. Foster, R. Gray, L. Badman, Sarah V Ray, E. J. Bunce, B. Snios,  
 921 C. M. Jackman, I. J. Rae, R. Kraft, S. Lathia, and N. Achilleos (in review),  
 922 Jupiter’s x-rays 2007 part 1: Jupiter’s x-ray emission during solar minimum,  
 923 *Journal of Geophysical Research: Space Physics*.
- 924 Ebert, R., D. McComas, F. Bagenal, and H. Elliott (2010), Location, structure, and  
 925 motion of jupiter’s dusk magnetospheric boundary from 1625 to 2550 rj, *Journal*  
 926 *of Geophysical Research: Space Physics*, *115*(A12).
- 927 Ebert, R. W., F. Bagenal, D. J. McComas, and C. M. Fowler (2014), A survey of  
 928 solar wind conditions at 5 au: a tool for interpreting solar wind-magnetosphere  
 929 interactions at jupiter, *Frontiers in Astronomy and Space Sciences*, *1*, 4.
- 930 Echer, E., P. Zarka, W. Gonzalez, A. Morioka, and L. Denis (2010), Solar wind  
 931 effects on jupiter non-io dam emissions during ulysses distant encounter (2003–  
 932 2004), *Astronomy & Astrophysics*, *519*, A84.
- 933 Elliott, H., D. McComas, P. Valek, G. Nicolaou, S. Weidner, and G. Livadiotis  
 934 (2016), The new horizons solar wind around pluto (swap) observations of the solar  
 935 wind from 11–33 au, *The Astrophysical Journal Supplement Series*, *223*(2), 19.
- 936 Elliott, H., P. Valek, D. McComas, P. Delamere, F. Bagenal, G. Gladstone, C. Olkin,  
 937 J. Spencer, S. Stern, L. Young, et al. (2018), Determining the alpha to proton  
 938 density ratio for the new horizons solar wind observations, *The Astrophysical*  
 939 *Journal*, *866*(2), 85.
- 940 Elliott, H. A., D. J. McComas, E. J. Zirnststein, B. M. Randol, P. A. Delamere, G. Li-  
 941 vadiotis, F. Bagenal, N. P. Barnes, S. A. Stern, L. A. Young, et al. (2019), Slowing  
 942 of the solar wind in the outer heliosphere, *The Astrophysical Journal*, *885*(2), 156.
- 943 Elsner, R. F., N. Lugaz, J. Waite, T. Cravens, G. Gladstone, P. Ford, D. Grodent,  
 944 A. Bhardwaj, R. MacDowall, M. Desch, et al. (2005), Simultaneous chandra x  
 945 ray, hubble space telescope ultraviolet, and ulysses radio observations of jupiter’s  
 946 aurora, *Journal of Geophysical Research: Space Physics (1978–2012)*, *110*(A1).
- 947 Forsyth, C., A. Fazakerley, I. Rae, C. Watt, K. Murphy, J. A. Wild, T. Karlsson,  
 948 R. Mutel, C. Owen, R. Ergun, et al. (2014), In situ spatiotemporal measurements  
 949 of the detailed azimuthal substructure of the substorm current wedge, *Journal of*  
 950 *Geophysical Research: Space Physics*, *119*(2), 927–946.
- 951 Gladstone, G., J. Waite, D. Grodent, W. Lewis, F. Crary, R. F. Elsner, M. Weis-  
 952 skopf, T. Majeed, J.-M. Jahn, A. Bhardwaj, et al. (2002), A pulsating auroral  
 953 x-ray hot spot on jupiter, *Nature*, *415*(6875), 1000–1003.
- 954 Gray, R., S. V. Badman, B. Bonfond, T. Kimura, H. Misawa, J. Nichols, M. Vogt,  
 955 and L. Ray (2016), Auroral evidence of radial transport at jupiter during january  
 956 2014, *Journal of Geophysical Research: Space Physics*, *121*(10), 9972–9984.
- 957 Grodent, D. (2015), A brief review of ultraviolet auroral emissions on giant planets,  
 958 *Space Science Reviews*, *187*(1-4), 23–50.
- 959 Grodent, D., B. Bonfond, J.-C. Gérard, A. Radioti, J. Gustin, J. T. Clarke,  
 960 J. Nichols, and J. E. Connerney (2008), Auroral evidence of a localized mag-  
 961 netic anomaly in jupiter’s northern hemisphere, *Journal of Geophysical Research:*  
 962 *Space Physics (1978–2012)*, *113*(A9).
- 963 Grodent, D., B. Bonfond, Z. Yao, J.-C. Gérard, A. Radioti, M. Dumont, B. Pal-  
 964 maerts, A. Adriani, S. V. Badman, E. Bunce, et al. (2018), Jupiter’s aurora ob-  
 965 served with hst during juno orbits 3 to 7, *Journal of Geophysical Research: Space*  
 966 *Physics*.



- 967 Guo, R., Z. Yao, Y. Wei, L. C. Ray, I. Rae, C. S. Arridge, A. Coates, P. Delamere,  
968 N. Sergis, P. Kollmann, et al. (2018a), Rotationally driven magnetic reconnection  
969 in saturn’s dayside, *Nature Astronomy*, p. 1.
- 970 Guo, R., Z. Yao, N. Sergis, Y. Wei, D. Mitchell, E. Roussos, B. Palmaerts, W. Dunn,  
971 A. Radioti, L. C. Ray, et al. (2018b), Reconnection acceleration in saturn’s day-  
972 side magnetodisk: A multicase study with cassini, *The Astrophysical Journal*  
973 *Letters*, 868(2), L23.
- 974 Gurnett, D., W. Kurth, G. Hospodarsky, A. Persoon, P. Zarka, A. Lecacheux,  
975 S. Bolton, M. Desch, W. Farrell, M. Kaiser, et al. (2002), Control of jupiter’s  
976 radio emission and aurorae by the solar wind, *Nature*, 415(6875), 985–987.
- 977 Gustin, J., B. Bonfond, D. Grodent, and J.-C. Gérard (2012), Conversion from hst  
978 acs and stis auroral counts into brightness, precipitated power, and radiated power  
979 for h2 giant planets, *Journal of Geophysical Research: Space Physics*, 117(A7).
- 980 Hess, S., B. Cecconi, and P. Zarka (2008), Modeling of io-jupiter decameter arcs,  
981 emission beaming and energy source, *Geophysical Research Letters*, 35(13).
- 982 Hess, S., P. Delamere, V. Dols, and L. Ray (2011), Comparative study of the power  
983 transferred from satellite-magnetosphere interactions to auroral emissions, *Journal*  
984 *of Geophysical Research: Space Physics*, 116(A1).
- 985 Hess, S., E. Echer, and P. Zarka (2012), Solar wind pressure effects on jupiter de-  
986 cametric radio emissions independent of io, *Planetary and Space Science*, 70(1),  
987 114–125.
- 988 Hess, S., E. Echer, P. Zarka, L. Lamy, and P. Delamere (2014), Multi-instrument  
989 study of the jovian radio emissions triggered by solar wind shocks and inferred  
990 magnetospheric subcorotation rates, *Planetary and Space Science*, 99, 136–148.
- 991 Hess, S. L., P. Delamere, V. Dols, B. Bonfond, and D. Swift (2010), Power trans-  
992 mission and particle acceleration along the io flux tube, *Journal of Geophysical*  
993 *Research: Space Physics*, 115(A6).
- 994 Hill, T. (2001), The jovian auroral oval, *Journal of Geophysical Research: Space*  
995 *Physics (1978–2012)*, 106(A5), 8101–8107.
- 996 Houston, S., T. Cravens, D. Schultz, H. Gharibnejad, W. Dunn, D. Haggerty,  
997 A. Rymer, B. Mauk, and N. Ozak (), Jovian auroral ion precipitation: X-ray  
998 production from oxygen and sulfur precipitation, *Journal of Geophysical Research:*  
999 *Space Physics*.
- 1000 Houston, S., N. Ozak, J. Young, T. Cravens, and D. Schultz (2018), Jovian auro-  
1001 ral ion precipitation: Field-aligned currents and ultraviolet emissions, *Journal of*  
1002 *Geophysical Research: Space Physics*, 123(3), 2257–2273.
- 1003 Jackman, C., C. Knigge, D. Altamirano, R. Gladstone, W. Dunn, R. Elsner,  
1004 R. Kraft, G. Branduardi-Raymont, and P. Ford (2018), Assessing quasi-  
1005 periodicities in jovian x-ray emissions: Techniques and heritage survey, *Journal*  
1006 *of Geophysical Research: Space Physics*, 123(11), 9204–9221.
- 1007 Jia, X., M. G. Kivelson, K. K. Khurana, and R. J. Walker (2010), Magnetic fields of  
1008 the satellites of jupiter and saturn, *Space science reviews*, 152(1-4), 271–305.
- 1009 Joy, S., M. Kivelson, R. Walker, K. Khurana, C. Russell, and T. Ogino (2002), Prob-  
1010 abilistic models of the jovian magnetopause and bow shock locations, *Journal of*  
1011 *Geophysical Research: Space Physics (1978–2012)*, 107(A10), SMP–17.
- 1012 Kimura, T., S. Badman, C. Tao, K. Yoshioka, G. Murakami, A. Yamazaki,  
1013 F. Tsuchiya, B. Bonfond, A. Steffl, A. Masters, et al. (2015), Transient inter-  
1014 nally driven aurora at jupiter discovered by hisaki and the hubble space telescope,  
1015 *Geophysical Research Letters*, 42(6), 1662–1668.
- 1016 Kimura, T., R. Kraft, R. Elsner, G. Branduardi-Raymont, G. Gladstone, C. Tao,  
1017 K. Yoshioka, G. Murakami, A. Yamazaki, F. Tsuchiya, et al. (2016), Jupiter’s  
1018 x-ray and euv auroras monitored by chandra, xmm-newton, and hisaki satellite,  
1019 *Journal of Geophysical Research: Space Physics*, 121(3), 2308–2320.

- 1020 Kita, H., T. Kimura, C. Tao, F. Tsuchiya, H. Misawa, T. Sakanoi, Y. Kasaba,  
 1021 G. Murakami, K. Yoshioka, A. Yamazaki, et al. (2016), Characteristics of solar  
 1022 wind control on jovian uv auroral activity deciphered by long-term hisaki exceed  
 1023 observations: Evidence of preconditioning of the magnetosphere?, *Geophysical*  
 1024 *Research Letters*, *43*(13), 6790–6798.
- 1025 Kivelson, M. G. (2004), Moon–magnetosphere interactions: a tutorial, *Advances in*  
 1026 *Space Research*, *33*(11), 2061–2077.
- 1027 Lamy, L., P. Zarka, B. Cecconi, L. Klein, S. Masson, L. Denis, A. Coffre, and  
 1028 C. Viou 1977 - 2017: 40 years of decametric observations of jupiter and the sun  
 1029 with the nançay decameter array, *Planetary Radio Emissions VIII*, pp. 455–466.
- 1030 Lamy, L., R. Prangé, K. Hansen, J. Clarke, P. Zarka, B. Cecconi, J. Aboudarham,  
 1031 N. André, G. Branduardi-Raymont, R. Gladstone, et al. (2012), Earth-based  
 1032 detection of uranus’ aurorae, *Geophysical Research Letters*, *39*(7).
- 1033 Leahy, D., W. Darbro, R. Elsner, M. Weisskopf, S. Kahn, P. Sutherland, and  
 1034 J. Grindlay (1983), On searches for pulsed emission with application to four  
 1035 globular cluster x-ray sources-ngc 1851, 6441, 6624, and 6712, *The Astrophysi-*  
 1036 *cal Journal*, *266*, 160–170.
- 1037 Lecacheux, A. (2000), The nançay decameter array: A useful step towards giant,  
 1038 new generation radio telescopes for long wavelength radio astronomy, *Radio As-*  
 1039 *tronomy at Long Wavelengths*, *119*, 321–328.
- 1040 Louis, C., L. Lamy, P. Zarka, B. Cecconi, M. Imai, W. Kurth, G. Hospodarsky,  
 1041 S. Hess, X. Bonnin, S. Bolton, et al. (2017), Io-jupiter decametric arcs observed by  
 1042 juno/waves compared to expres simulations, *Geophysical Research Letters*, *44*(18),  
 1043 9225–9232.
- 1044 Louis, C. K., Hess, S. L. G., Cecconi, B., Zarka, P., Lamy, L., Aicardi, S., and Loh,  
 1045 A. (2019), Expres: an exoplanetary and planetary radio emissions simulator,  
 1046 *A&A*, *627*, A30, doi:10.1051/0004-6361/201935161.
- 1047 Ma, X., P. Delamere, A. Otto, and B. Burkholder (2017), Plasma transport driven  
 1048 by the three-dimensional kelvin-helmholtz instability, *Journal of Geophysical Re-*  
 1049 *search: Space Physics*, *122*(10), 10–382.
- 1050 MacDowall, R., M. Kaiser, M. Desch, W. Farrell, R. Hess, and R. Stone (1993),  
 1051 Quasiperiodic jovian radio bursts: Observations from the ulysses radio and plasma  
 1052 wave experiment, *Planetary and space science*, *41*(11), 1059–1072.
- 1053 Manners, H., A. Masters, and J. Yates (2018), Standing alfvén waves in jupiter’s  
 1054 magnetosphere as a source of 10-to 60-min quasiperiodic pulsations, *Geophysical*  
 1055 *Research Letters*, *45*(17), 8746–8754.
- 1056 Marques, M., P. Zarka, E. Echer, V. Ryabov, M. Alves, L. Denis, and A. Coffre  
 1057 (2017), Statistical analysis of 26 yr of observations of decametric radio emissions  
 1058 from jupiter, *Astronomy & Astrophysics*, *604*, A17.
- 1059 Mauk, B., J. Clarke, D. Grodent, J. Waite, C. Paranicas, and D. Williams (2002),  
 1060 Transient aurora on jupiter from injections of magnetospheric electrons, *Nature*,  
 1061 *415*(6875), 1003–1005.
- 1062 Mauk, B., D. Haggerty, C. Paranicas, G. Clark, P. Kollmann, A. Rymer,  
 1063 D. Mitchell, S. Bolton, S. Levin, A. Adriani, et al. (2017), Juno observations of  
 1064 energetic charged particles over jupiter’s polar regions: Analysis of monodirec-  
 1065 tional and bidirectional electron beams, *Geophysical Research Letters*, *44*(10),  
 1066 4410–4418.
- 1067 Mauk, B. H., and J. Saur (2007), Equatorial electron beams and auroral structuring  
 1068 at jupiter, *Journal of Geophysical Research: Space Physics*, *112*(A10).
- 1069 McComas, D., and F. Bagenal (2007), Jupiter: A fundamentally different magneto-  
 1070 spheric interaction with the solar wind, *Geophysical Research Letters*, *34*(20).
- 1071 McComas, D., F. Allegrini, F. Bagenal, F. Crary, R. Ebert, H. Elliott, A. Stern, and  
 1072 P. Valek (2007), Diverse plasma populations and structures in jupiter’s magneto-  
 1073 tail, *science*, *318*(5848), 217–220.

- 1074 McComas, D., F. Allegrini, F. Bagenal, P. Casey, P. Delamere, D. Demkee, G. Dunn,  
1075 H. Elliott, J. Hanley, K. Johnson, et al. (2008), The solar wind around pluto  
1076 (swap) instrument aboard new horizons, *Space Science Reviews*, *140*(1-4), 261–  
1077 313.
- 1078 McComas, D., H. Elliott, S. Weidner, P. Valek, E. Zirnstein, F. Bagenal, P. De-  
1079 lamere, R. Ebert, H. Funsten, M. Horanyi, et al. (2016), Pluto’s interaction with  
1080 the solar wind, *Journal of Geophysical Research: Space Physics*, *121*(5), 4232–  
1081 4246.
- 1082 Nichols, J., J. Clarke, J.-C. Gérard, and D. Grodent (2009a), Observations of jovian  
1083 polar auroral filaments, *Geophysical Research Letters*, *36*(8).
- 1084 Nichols, J., J. Clarke, J.-C. Gérard, D. Grodent, and K. Hansen (2009b), Varia-  
1085 tion of different components of jupiter’s auroral emission, *Journal of Geophysical*  
1086 *Research: Space Physics* (1978–2012), *114*(A6).
- 1087 Nichols, J., S. V. Badman, F. Bagenal, S. Bolton, B. Bonfond, E. Bunce, J. Clarke,  
1088 J. Connerney, S. Cowley, R. Ebert, et al. (2017a), Response of jupiter’s auro-  
1089 ras to conditions in the interplanetary medium as measured by the hubble space  
1090 telescope and juno, *Geophysical Research Letters*, *44*(15), 7643–7652.
- 1091 Nichols, J., T. Yeoman, E. Bunce, M. Chowdhury, S. Cowley, and T. Robinson  
1092 (2017b), Periodic emission within jupiter’s main auroral oval, *Geophysical Re-*  
1093 *search Letters*, *44*(18), 9192–9198.
- 1094 Nicolaou, G., D. McComas, F. Bagenal, and H. Elliott (2014), Properties of plasma  
1095 ions in the distant jovian magnetosheath using solar wind around pluto data on  
1096 new horizons, *Journal of Geophysical Research: Space Physics*, *119*(5), 3463–3479.
- 1097 Nicolaou, G., D. McComas, F. Bagenal, H. Elliott, and R. Ebert (2015), Jupiter’s  
1098 deep magnetotail boundary layer, *Planetary and Space Science*, *111*, 116–125.
- 1099 Owens, M. J., and R. J. Forsyth (2013), The heliospheric magnetic field, *Living*  
1100 *Reviews in Solar Physics*, *10*(1), 5.
- 1101 Pallier, L., and R. Prangé (2001), More about the structure of the high latitude  
1102 jovian aurorae, *Planetary and Space Science*, *49*(10), 1159–1173.
- 1103 Pallier, L., and R. Prangé (2004), Detection of the southern counterpart of the jo-  
1104 vian northern polar cusp: Shared properties, *Geophysical research letters*, *31*(6).
- 1105 Paranicas, C., B. Mauk, D. Haggerty, G. Clark, P. Kollmann, A. Rymer, B. Bon-  
1106 fond, W. Dunn, R. Ebert, G. Gladstone, et al. (2018), Intervals of intense ener-  
1107 getic electron beams over jupiter’s poles, *Journal of Geophysical Research: Space*  
1108 *Physics*, *123*(3), 1989–1999.
- 1109 Prangé, R., P. Zarka, G. Ballester, T. Livengood, L. Denis, T. Carr, F. Reyes,  
1110 S. Bame, and H. Moos (1993), Correlated variations of uv and radio emissions  
1111 during an outstanding jovian auroral event, *Journal of Geophysical Research:*  
1112 *Planets* (1991–2012), *98*(E10), 18,779–18,791.
- 1113 Prangé, R., L. Pallier, K. C. Hansen, R. Howard, A. Vourlidas, R. Courtin, and  
1114 C. Parkinson (2004), An interplanetary shock traced by planetary auroral storms  
1115 from the sun to saturn, *Nature*, *432*(7013), 78–81.
- 1116 Radioti, A., D. Grodent, J.-C. Gérard, M. Vogt, M. Lystrup, and B. Bonfond (2011),  
1117 Nightside reconnection at jupiter: Auroral and magnetic field observations from 26  
1118 july 1998, *Journal of Geophysical Research: Space Physics*, *116*(A3).
- 1119 Saur, J., F. M. Neubauer, J. Connerney, P. Zarka, and M. G. Kivelson (2004),  
1120 Plasma interaction of io with its plasma torus, *Jupiter: The Planet, Satellites*  
1121 *and Magnetosphere*, *1*, 537–560.
- 1122 Shi, Q., M. Hartinger, V. Angelopoulos, A. Tian, S. Fu, Q.-G. Zong, J. Weygand,  
1123 J. Raeder, Z. Pu, X. Zhou, et al. (2014), Solar wind pressure pulse-driven magne-  
1124 tospheric vortices and their global consequences, *Journal of Geophysical Research:*  
1125 *Space Physics*, *119*(6), 4274–4280.
- 1126 Sinclair, J., G. Orton, J. Fernandes, Y. Kasaba, T. Sato, T. Fujiyoshi, C. Tao,  
1127 M. Vogt, D. Grodent, B. Bonfond, et al. (2019), A brightening of jupiter’s au-

- 1128 roral 7.8- $\mu\text{m}$  ch 4 emission during a solar-wind compression, *Nature Astronomy*,  
 1129 p. 1.
- 1130 Smith, R., A. Foster, and N. Brickhouse (2012), Approximating the x-ray spectrum  
 1131 emitted from astrophysical charge exchange, *Astronomische Nachrichten*, *333*(4),  
 1132 301–304.
- 1133 Southwood, D., and M. Kivelson (2001), A new perspective concerning the influence  
 1134 of the solar wind on the jovian magnetosphere, *Journal of Geophysical Research:*  
 1135 *Space Physics (1978–2012)*, *106*(A4), 6123–6130.
- 1136 Stallard, T., S. Miller, S. Cowley, and E. Bunce (2003), Jupiter’s polar ionospheric  
 1137 flows: Measured intensity and velocity variations poleward of the main auroral  
 1138 oval, *Geophysical research letters*, *30*(5).
- 1139 Stallard, T. S., J. T. Clarke, H. Melin, S. Miller, J. D. Nichols, J. O’Donoghue,  
 1140 R. E. Johnson, J. E. Connerney, T. Satoh, and M. Perry (2016), Stability within  
 1141 jupiter’s polar auroral ‘swirl region’ over moderate timescales, *Icarus*, *268*, 145–  
 1142 155.
- 1143 Szalay, J., B. Bonfond, F. Allegrini, F. Bagenal, S. Bolton, G. Clark, J. Connerney,  
 1144 R. Ebert, R. Ergun, G. Gladstone, et al. (2018), In situ observations connected  
 1145 to the io footprint tail aurora, *Journal of Geophysical Research: Planets*, *123*(11),  
 1146 3061–3077.
- 1147 Tao, C., R. Kataoka, H. Fukunishi, Y. Takahashi, and T. Yokoyama (2005),  
 1148 Magnetic field variations in the jovian magnetotail induced by solar wind dy-  
 1149 namic pressure enhancements, *Journal of Geophysical Research: Space Physics*,  
 1150 *110*(A11).
- 1151 Vogt, M. F., E. J. Bunce, M. G. Kivelson, K. K. Khurana, R. J. Walker, A. Radi-  
 1152 oti, B. Bonfond, and D. Grodent (2015), Magnetosphere-ionosphere mapping at  
 1153 jupiter: Quantifying the effects of using different internal field models, *Journal of*  
 1154 *Geophysical Research: Space Physics*.
- 1155 Von Steiger, R., N. Schwadron, L. Fisk, J. Geiss, G. Gloeckler, S. Hefti, B. Wilken,  
 1156 R. Wimmer-Schweingruber, and T. Zurbuchen (2000), Composition of quasi-  
 1157 stationary solar wind flows from ulysses/solar wind ion composition spectrometer,  
 1158 *Journal of Geophysical Research: Space Physics*, *105*(A12), 27,217–27,238.
- 1159 Watanabe, H., H. Kita, C. Tao, M. Kagitani, T. Sakanoi, and Y. Kasaba (2018),  
 1160 Pulsation characteristics of jovian infrared northern aurora observed by the subaru  
 1161 ircs with adaptive optics, *Geophysical Research Letters*, *45*(21), 11–547.
- 1162 Yao, Z., A. Coates, L. Ray, I. Rae, D. Grodent, G. H. Jones, M. Dougherty,  
 1163 C. Owen, R. Guo, W. Dunn, et al. (2017), Corotating magnetic reconnection  
 1164 site in saturn’s magnetosphere, *The Astrophysical Journal Letters*, *846*(2), L25.
- 1165 Yates, J., N. Achilleos, and P. Guio (2014), Response of the jovian thermosphere to  
 1166 a transient ‘pulse’ in solar wind pressure, *Planetary and Space Science*, *91*, 27–44.
- 1167 Zarka, P. (1998), Auroral radio emissions at the outer planets: Observations and  
 1168 theories, *Journal of Geophysical Research: Planets (1991–2012)*, *103*(E9), 20,159–  
 1169 20,194.
- 1170 Zhao, H., X. Shen, B. Tang, A. Tian, Q. Shi, J. Weygand, Z. Yao, Q.-G. Zong,  
 1171 S. Fu, S. Yao, et al. (2016), Magnetospheric vortices and their global effect after  
 1172 a solar wind dynamic pressure decrease, *Journal of Geophysical Research: Space*  
 1173 *Physics*, *121*(2), 1071–1077.
- 1174 Zieger, B., and K. C. Hansen (2008), Statistical validation of a solar wind propa-  
 1175 gation model from 1 to 10 au, *Journal of Geophysical Research: Space Physics*  
 1176 *(1978–2012)*, *113*(A8).